Title: ATRAID, a genetic factor that regulates the action of nitrogen-containing bisphosphonates on bone

Authors: Lauren E. Surface[1,&], Damon T. Burrow[2], Jinmei Li[2], Jiwoong Park[2], Sandeep Kumar[2], Cheng Lyu[2], Niki Song[2], Zhou Yu[1,^], Abbhirami Rajagopal[3,#], Yangjin Bae[3], Brendan H. Lee[3], Steven Mumm[2], Charles C. Gu[4], Jonathan C. Baker[5], Mahshid Mohseni[2], Melissa Sum[6], Margaret Huskey[2], Shenghui Duan[2], Vinieth N. Bijanki[7], Roberto Civitelli[2], Michael J. Gardner[8], Chris M. McAndrew[9], William M. Ricci[10], Christina A. Gurnett[9,11], Kathryn Diemer[2], Fei Wan[12], Christina L. Costantino[13], Kristen M. Shannon[14], Noopur Raje[14], Thomas B. Dodson[15,@], Daniel A. Haber[14,16], Jan E. Carette[17], Malini Varadarajan[18,*], Thijn R. Brummelkamp[18], Kivanc Birsoy[19], David M. Sabatini[16,20-22], Gabe Haller[11,23], Timothy R. Peterson[2,24,25]*

Affiliations:

[1] Department of Molecular and Cellular Biology, Department of Chemistry and Chemical Biology, Faculty of Arts and Sciences Center for Systems Biology, Harvard University, Cambridge, MA 02138, USA.

[&] (present address) Endocrine Unit, 55 Fruit St., Massachusetts General Hospital, Harvard Medical School, Boston, MA, 02114, USA.

[^] (present address) Howard Hughes Medical Institute (HHMI) Janelia Research Campus, 19700 Helix Drive, Ashburn, Virginia 20147, USA.

[2] Division of Bone & Mineral Diseases, Department of Medicine, Washington University School of Medicine, BJC Institute of Health, 425 S. Euclid Ave., St. Louis, MO 63110, USA.

[3] Department of Molecular and Human Genetics, Baylor College of Medicine, Houston, TX, 77030, USA.

[#] (present address) Harris County Public health, Houston, TX, 77027, USA.

[4] Division of Biostatistics, Washington University School of Medicine, 660 S. Euclid Ave., Campus Box 8067, St. Louis, MO 63110, USA.

[5] Mallinckrodt Institute of Radiology, Washington University School of Medicine, 510 S. Kingshighway Blvd. Louis, MO 63110, USA.

[6] Division of Endocrinology, Diabetes and Metabolism, NYU Langone Health, 530 1st Ave., Schwartz 5E. New York, NY 10016, USA.

[7] Center for Metabolic Bone Disease and Molecular Research, Shriners Hospital for Children, St. Louis, MO 63110, USA.

[8] Stanford University, Department of Orthopedic Surgery, 450 Broadway Street, Redwood City, CA 94063, USA.

[9] Department of Orthopedic Surgery, Washington University School of Medicine, 4938 Parkview Place, St. Louis, MO 63110, USA.

[10] Hospital for Special Surgery Main Campus - Belaire Building, 525 East 71st Street 2nd Floor, New York, NY 10021, USA.

[11] Department of Neurology, Washington University School of Medicine, Campus Box 8111, 660 S. Euclid Ave., St. Louis, MO 63110, USA.

[12] Department of Surgery, Washington University School of Medicine, Campus Box 8109, 4590 Children's Place, Suite 9600, St. Louis, MO 63110, USA.

[13] Massachusetts General Hospital Cancer Center and Department of Surgery, Harvard Medical School, Boston, MA 02114, USA.

[14] Massachusetts General Hospital Cancer Center, Harvard Medical School, Boston, MA 02114, USA.

[15] Department of Oral and Maxillofacial Surgery, Massachusetts General Hospital and Harvard Medical School, Boston, MA 02114, USA.
[@] (present address) University of Washington, Seattle, WA 98195, USA.
[16] Howard Hughes Medical Institute (HHMI), Chevy Chase, MD 20815, USA.
[17] Department of Microbiology and Immunology, Stanford University School of Medicine, Stanford, CA 94305, USA.
[18] Netherlands Cancer Institute, Amsterdam, The Netherlands.
[*] (present address) Developmental and molecular pathways, Novartis institutes for biomedical research, Cambridge, CA 02140, USA.
[19] The Rockefeller University, 1230 York Ave, New York 10065, USA.
[20] Whitehead Institute, 9 Cambridge Center, Cambridge, MA 02139, USA.
[21] Department of Biology, Massachusetts Institute of Technology (MIT), 77 Massachusetts Avenue, Cambridge, MA 02139, USA.
[22] David H. Koch Center for Integrative Cancer Research at MIT, 77 Massachusetts Avenue, Cambridge, MA 02139, USA.
[23] Department of Neurosurgery, Washington University School of Medicine, Campus Box 8057, 660 S. Euclid Ave., St. Louis, MO 63110, USA.
[24] Department of Genetics, Washington University School of Medicine, 4515 McKinley Ave. Campus Box 8232, St. Louis, MO 63110, USA.
[25] Institute for Public Health, Washington University School of Medicine, 600 S. Taylor Suite 2400, Campus Box 8217, St. Louis, MO 63110, USA.
Corresponding author:[::] * timrpeterson@wustl.edu (T.R.P).

One Sentence Summary: The identification of the gene, *ATRAID*, essential for responses to the commonly prescribed osteoporosis drugs, nitrogen-containing bisphosphonates.

Abstract:

Nitrogen-containing bisphosphonates (N-BPs), such as alendronate (Fosamax®), are the mostly widely prescribed medications for diseases involving bone (*1-3*), with nearly 200 million prescriptions written annually. In the last few years, widespread use of N-BPs has been challenged due to the risk of rare but significant side effects such as atypical femoral fractures (AFF) and osteonecrosis of the jaw (ONJ) (*4-7*). N-BPs bind to and inhibit farnesyl diphosphate synthase (FDPS), resulting in defects in protein prenylation (*8-10*). Yet it remains poorly understood what other cellular factors might allow N-BPs to exert their pharmacological effects. Herein, we perform genome-wide studies in cells and patients to identify the poorly characterized gene, *ATRAID*. Loss of *ATRAID* function results in selective resistance to N-BP-mediated loss of cell viability and the prevention

of alendronate-mediated inhibition of prenylation. *ATRAID* is required for alendronate inhibition of osteoclast function, and *ATRAID*-deficient mice have impaired therapeutic responses to alendronate in both postmenopausal and senile (old age) osteoporosis models. Lastly, we performed exome sequencing on patients taking N-BPs that suffered ONJ or an AFF. *ATRAID* is one of three genes that contain rare non-synonymous coding variants in the ONJ and AFF patients that is also differentially expressed in poor outcome groups of patients treated with N-BPs. We functionally validated this patient variation in *ATRAID* as conferring cellular hypersensitivity to N-BPs. Our work adds key insight into the mechanistic action of N-BPs and the processes that might underlie differential responsiveness to N-BPs in people.

INTRODUCTION

Nitrogen-containing bisphosphonates (N-BPs) are the standard treatment for osteoporosis and several other bone diseases (*11, 12*). Certain N-BPs (pamidronate (Aredia®), zoledronate (Zometa®)) are also routinely prescribed to prevent skeletal complications in patients with multiple myeloma and with bone metastases from other malignancies, including breast and prostate cancer (*13*). However, because N-BPs cause rare yet serious side-effects, such as atypical fractures and osteonecrosis of the jaw, many patients avoid taking them (*5-7, 11*), causing the number of prescriptions to plummet over 50% in the last decade (*7, 14*). A plan for addressing this crisis, developed by American Society for Bone and Mineral Research (ASBMR) leadership, calls for better pharmacogenomics to identify genetic factors that may underlie response to this class of drugs (*7*).

A goal of personalized medicine is to identify biomarkers that underlie drug responsiveness. In the case of the N-BPs, it can be said that there are limited personalization options owing to the limited number of genes implicated in the pharmacologic effects of N-BPs. Exposure of cells to N-BPs leads to inhibition of farnesyl diphosphate synthase (FDPS, a.k.a., FPPS) resulting in reduction in protein prenylation (*15*). Based on this observation, it is widely believed that N-BPs act therapeutically by impairing protein prenylation, ultimately leading to deficits in numerous cellular processes including differentiation, recruitment, and adhesion of osteoclasts (the major bone resorptive cell type) to bone and/or osteoclast cell death (*16-18*). Recently we performed CRISPRi-based, genome-wide screening and identified a poorly characterized gene, *SLC37A3,* that provides molecular details for how N-BPs reach their target, FDPS (*19*). As part of that work we determined that SLC37A3 requires another poorly characterized protein, ATRAID, for its expression (*19*). In this work, we independently identified *ATRAID* using a different genome-wide, mutagenesis strategy. We generated *ATRAID* deficient mice and determined that it is required for the regulation of N-BPs on bone. We also performed exome sequencing in patients

taking N-BPs and identified and functionally validated rare coding variants in *ATRAID* in patients that suffered side effects, namely atypical femoral fractures and osteonecrosis of the jaw.

RESULTS

ATRAID is required for molecular responses to nitrogen-containing bisphosphonates

To provide insight into the mechanism(s) of N-BPs action, we performed a genetic screen to identify human genes required for the anti-proliferative effects of N-BPs (Fig. 1A). We made use of a largely haploid human cell line of myeloid origin (KBM7, a.k.a. HAP1) to generate a library of retroviral gene trap mutants (*20*), and then selected for clones which are resistant to cytotoxic levels of alendronate (ALN). The advantages of this cell line for genetic screening include: 1) each gene is present as a single copy, enabling gene inactivation (except those genes on chromosome 8); 2) KBM7 cells are human and of the hematopoietic lineage, increasing the likelihood that any genes we identify could be relevant to the natural context for N-BPs, the bones of human patients (*21*); and 3) it is a different cell line and a different mutagenic approach than that we used with CRISPRi in K562 cells (*19*), which allows us to independently assess those results. Using this haploid approach, we identified, *ATRAID*, a.k.a., *APR-3/C2orf28* (*22*), as the gene most significantly enriched for insertions in alendronate resistant cells compared to untreated cells (Fig. 1B; fig. S1, A and B, and table S1). Providing confidence in our screen, we also identified *SLC37A3* as well as *SNTG1*, *PLCL1*, and *EPHB1,* which have been previously connected to N-BP action on bone cells and/or human bone diseases (table S1) (*23-25*).

ATRAID was named because it is a gene whose mRNA expression is strongly induced by the ligand, all-trans retinoic acid (*22*). *ATRAID* is conserved in chordates and contains a signal peptide, Toll-like-receptor leucine rich repeat, EGF-like domain, and a transmembrane domain (Fig. 1C and fig. S1A) (*26, 27*). Importantly, the alendronate resistance phenotype of *ATRAID* deficient cells (ATRAID_GT1 (gene-trap1) and ATRAID_GT2 (gene-trap2)) was reversed by the

151 re-introduction of wild-type *ATRAID* splice variant 2 (v2) or splice variant 3 (v3) cDNA, which
152 differ in their N-termini (Fig. 1D; fig. S1, A and B). To better understand the level of alendronate
153 resistance in *ATRAID* deficient cells, we varied both cell number and drug concentration in the
154 viability assay. *ATRAID* deficient cells were resistant to alendronate over two to three orders of
155 magnitude of drug concentration or cell number (fig. S1C). The growth of untreated wild-type
156 and *ATRAID* deficient cells didn't differ (fig. S1D). Overexpression of full-length ATRAID (v2)
157 sensitized cells to alendronate (fig. S1E). Lastly, ATRAID membrane targeting is required for the
158 anti-proliferative effects of alendronate, as *ATRAID* deficient cells complemented with full-length
159 ATRAID (v2) were sensitive to the cytotoxic effects of alendronate, whereas those expressing
160 the membrane truncated form remained resistant (fig. S1F). Taken together, these data
161 establish *ATRAID* as a genetic factor required for the growth inhibitory effects of alendronate.
162
163 N-BPs are part of a larger class of compounds known as bisphosphonates (BPs) that contain
164 two phosphate moieties each joined to a carbon atom by a carbon-phosphorus bond (*28*) (Fig.
165 1E). To determine whether the effects of *ATRAID* deficiency on alendronate resistance were
166 specific to nitrogen-containing bisphosphonates, we tested the effect of several nitrogen-
167 containing and non-nitrogen-containing bisphosphonates on wild-type and mutant *ATRAID* cells.
168 *ATRAID* deficient cells were resistant to the nitrogen-containing bisphosphonates, alendronate
169 and zoledronate (ZOL), but were as sensitive to the non-nitrogen-containing bisphosphonates,
170 etidronate and tiludronate, as control cells (Fig. 1E).
171
172 To determine whether *ATRAID* is required for the reduction in protein prenylation observed
173 upon N-BP treatment, we monitored the prenylation of several proteins, including the heat shock
174 protein DnaJ (Hsp40) homolog HDJ-2, and the Ras family GTPase Rap1a (*29*). Alendronate
175 strongly inhibited prenylation of HDJ-2 and Rap1a in wild-type cells in a dose dependent
176 manner and had much less of an effect on prenylation of these proteins in *ATRAID* deficient

177 cells (Fig. 1F). Furthermore, the inhibitory effect of alendronate on prenylation was rescued
178 when *ATRAID* cDNA variants (v2 and v3) were introduced (fig. S1F). We observed inhibition of
179 prenylation resistance at N-BP doses where we did not see PARP-1 cleavage in *ATRAID*
180 deficient cells, suggesting that *ATRAID* can mediate the effect on prenylation independent of
181 apoptosis (fig. S1G). Thus, these findings suggest *ATRAID* functions as a positive regulator
182 upstream of FDPS.
183
184 **ATRAID is required for organismal responses to nitrogen-containing bisphosphonates**
185 To determine whether ATRAID modulates organismal responses to N-BPs we inactivated
186 *ATRAID* globally in mice (*30*). We confirmed deletion of *ATRAID* exons 3-5 and determined that
187 *ATRAID* homozygous deleted *ATRAID*^{KO} mice (labeled KO, -/-) are viable but their body weight
188 is mildly reduced compared with litter-matched derived, wild-type controls (labeled as WT, +/+)
189 (fig. S2A-C). We confirmed that tail fibroblasts derived from *ATRAID*^{KO} animals are resistant to
190 the cytotoxic effects of alendronate (fig. S2, D and E). Before studying the effects of the N-BPs
191 in the context of *ATRAID* loss, we first characterized the basal role of *ATRAID* in bones. We
192 determined that *ATRAID* mRNA expression was undetectable in the bones of *ATRAID*^{KO}
193 animals and that *ATRAID*^{KO} mice had slightly smaller bones compared with litter-matched
194 derived, wild-type control mice (fig. S2, F and G). To examine the effects of *ATRAID* on bone
195 structure, we performed micro-computed tomography (μCT) analysis (*31*). *ATRAID* deficiency
196 did not significantly decrease either trabecular and cortical structural parameters (fig. S2, H and
197 I; table S2). We measured bone strength using three-point bending tests (*32*). Some measures,
198 such as stiffness (Newtons/millimeter, N/mm) and post-yield displacement (a measure of bone
199 fragility, in millimeters, mm) were decreased by *ATRAID* deficiency, whereas others, such as
200 yield load (the point where bone bending goes from elastic vs. plastic, in Newtons, N), were not
201 significantly altered (fig. S2, J-L; table S2).
202

203 Osteoclasts release degradation products from C-terminal telopeptides of type I collagen (CTX-
204 I) from bone into blood (*33*), and levels of CTX-I in serum were not significantly different in wild-
205 type mice compared with *ATRAID*^{KO} mice (fig. S2M; table S2). Histomorphometric measures of
206 osteoclast function including osteoclast surface per bone surface (Oc.S/BS) (*34*), as judged by
207 Tartrate Resistant Acid Phosphatase (TRAP) staining (*35*), were also not statistically different
208 (fig. S2N; table S2). Consistent with a basal defect in osteoblast function (*36*), *ATRAID*^{KO} mice
209 have reduced serum levels of circulating Gla-Osteocalcin (Gla-OC; the activated form of
210 osteocalcin, incorporated in bone matrix (*37*)) and modestly reduced bone formation rate (BFR)
211 as measured by double-labeling (*34*) (fig. S2, O and P; table S2).
212
213 To test the effect of alendronate in a model that mimics menopausal bone loss, the most
214 common indication for the N-BPs, we performed ovariectomies (OVX) on adult female mice
215 (Fig. 2A) (*38*). When ovaries are removed from females, the changes in estrogen cause a
216 reduction in bone density triggered by disruption of the balance of osteoblast and osteoclast
217 functions. This loss of bone density can be alleviated by treatment with N-BPs (*39*). The
218 magnitude of trabecular bone loss in WT and *ATRAID*^{KO} sham mice four weeks after OVX is
219 exemplified in the μCT 3D reconstruction of the femoral proximal metaphysis (Fig. 2B).
220 Consistent with alendronate preventing bone loss (*39*), femoral cortical and trabecular structural
221 parameters, including cortical thickness and area, bone volume/trabecular volume (%) and
222 trabecular thickness, were increased by alendronate treatment of WT OVX mice (Fig. 2, C-F
223 and table S2; see WT OVX +/- alendronate). In contrast, alendronate had blunted effects in
224 *ATRAID*^{KO} OVX mice (Fig. 2, C-F and table S2; see *ATRAID*^{KO} OVX +/- alendronate).
225
226 The same patterns of alendronate resistance in *ATRAID*^{KO} mice were observed for bone
227 strength (Fig. 2, G and H). That is, alendronate increased bone strength as judged by stiffness
228 and yield load in wild-type ovariectomized mice, but its effects were significantly blunted in

229 *ATRAID*^{KO} matched cohorts (Fig. 2, G and H; table S2). Taken together, these results suggest
230 that ATRAID is required for the beneficial bone effects of N-BPs in ovariectomized female mice.
231
232 To test an additional osteoporosis model, we examined senile (i.e., old age) osteoporosis using
233 18 month-old male WT and *ATRAID* deficient mice (*40*). After treating these mice weekly with
234 alendronate or saline for two months, we found similar results to those in our OVX study. That
235 is, measures of bone density were increased by alendronate, but less so in the *ATRAID*
236 deficient mice (fig. S2, Q and R, table S2). This further suggests ATRAID is key for responses to
237 N-BPs in vivo.
238
239 **ATRAID is required cell-autonomously for N-BP inhibition of osteoclast function**
240 Because N-BPs potentially affect osteoclasts and osteoblasts, we investigated whether ATRAID
241 deficiency would regulate the effects of alendronate in each cell type in our osteoporosis
242 models, post-menopausal (OVX) and old-age (senile). Regarding osteoclasts, in wild-type mice
243 both serum and bone histological markers of osteoclast function, CTX-I, and osteoclast surface
244 per bone surface (Oc.S/BS) and osteoclast number per bone surface (N.Oc/BS), respectively,
245 were impaired by alendronate treatment (Fig. 3, A and B; fig. S3, A and B; table S3) in both
246 osteoporosis models. In contrast, in *ATRAID*^{KO} mice, alendronate was less effective on
247 osteoclasts in both osteoporosis models (Fig. 3, A and B; fig. S3, A and B; table S3). That
248 osteoclast number was reduced by N-BPs in wild-type mice is consistent with our cell viability
249 measurements in non-osteoclasts (Fig. 1; fig. S1, S2) and with previous literature (*39*).
250
251 To provide insight into the effects of N-BPs on osteoblasts in our osteoporosis models, we
252 measured BFR and mineral apposition rate (MAR) (*34*). Unlike BFR where the bone formation
253 rate is normalized by the amount of labeled bone surface, MAR is the rate of bone formation
254 irrespective of how much of the bone is active (*34*). Alendronate did not affect trabecular MAR

255 or BFR in either wild-type or *ATRAID*^{KO} mice in either osteoporosis model (fig. S3, C and D;
256 table S3).
257
258 To determine whether *ATRAID* is required in a cell autonomous manner for the N-BP-
259 dependent effects on osteoclasts, we isolated M-CSF expanded, bone marrow macrophages
260 (BMMs) from both WT and ATRAID^{KO} mice, and differentiated these cells into osteoclasts
261 following a standard protocol (*41*). *ATRAID*^{KO} BMMs differentiated into osteoclasts as well as
262 wild-type cells irrespective of treatment with alendronate, yet BMM-derived *ATRAID*^{KO}
263 osteoclasts were resistant to alendronate-induced apoptosis (Fig. 3, C and D). This suggests
264 that *ATRAID* is required cell autonomously in osteoclasts for the effects of N-BPs on cell
265 number.
266
267 As an independent confirmation of our primary cell experiments, we generated *ATRAID*
268 knockout RAW 264.7 cells and differentiated them to osteoclasts (fig. S3E). RAW 264.7 cells
269 are a robust, well-characterized murine macrophage cell line that can be differentiated to
270 osteoclast-like cells using RANKL (*42*). We treated both RAW 264.7 cells and the RAW 264.7
271 cells differentiated into osteoclasts with alendronate, and found *ATRAID* deficiency, as
272 expected, conferred resistance to doses that induced apoptosis (Fig. 3E). Alendronate did not
273 affect known markers of osteoclast differentiation in wild-type cells (Fig. 3C). Therefore, to
274 pursue the mechanism of N-BPs on osteoclast function, we focused on prenylation. In
275 alendronate-treated RAW 264.7 and differentiated RAW 264.7 to osteoclast cells, we found
276 *ATRAID*^{KO} cells were resistant to alendronate-induced inhibition of prenylation (Fig. 3F).
277
278 We assessed whether wild-type osteoblasts might sensitize *ATRAID* deficient osteoclasts to N-
279 BPs. We cultured primary wild-type osteoblasts with either WT or *ATRAID* deficient primary
280 osteoclasts and treated these co-cultures with alendronate or vehicle. As in the case of WT

281 RAW 264.7 cells grown independently (Fig. 3, E and F), WT osteoclasts were significantly more
282 affected by alendronate than *ATRAID* deficient osteoclasts despite the presence of WT
283 osteoblasts in both cases (Fig. 3, G and H). In total, these findings suggest that ATRAID is
284 required for the cell-autonomous effects of N-BPs on osteoclasts.
285

286 **Genetic factors involved in responses to nitrogen-containing bisphosphonates in**
287 **patients**

288 We sought an unbiased approach to determine what genes might be relevant in patients treated
289 with N-BPs. We performed whole exome sequencing (WES) on two sets of patients taking N-
290 BPs who experienced side effects: osteoporotic patients who experienced atypical femoral
291 fractures (AFF) (n = 27 patients) as well as multiple myeloma and breast cancer patients who
292 experienced osteonecrosis of the jaw (ONJ) (n = 8 patients) and 11 control patients taking N-
293 BPs that didn't experience AFF or ONJ (Fig. 4A and table S4 for patient information; see also
294 Materials and Methods for details on how these datasets were generated and analyzed). We
295 also analyzed two published gene expression datasets involving patients who had taken N-BPs:
296 multiple myeloma patients who did or did not suffer ONJ when taking N-BPs (*43*); and breast
297 cancer patients with bone marrow disseminated tumor cells (DTC) which reoccurred or the
298 patient died less than 1000 days vs. greater than 2500 days following initiation of zoledronate
299 treatment (*44*) (Fig. 4A and table S4). We then compared the patient data to three cell-based,
300 genome-wide CRISPRi and CRISPRa screens we previously performed: alendronate and
301 zolendronate CRISPRi and alendronate CRISPRa (*19, 45*) (table S4). To identify genes
302 involved in N-BP response across experimental paradigms we generated a Venn diagram to
303 visualize the overlap of "hits". In comparing the WES hits – i.e., genes that had the same rare
304 coding variants (minor allele frequency < 0.05) in both AFF and ONJ patients but not in controls
305 – with our hits from our alendronate and zoledronate CRISPRi/a screens we identified 64 genes
306 in common including *ATRAID, FDPS,* and *SLC37A3* (Fig. 4A). When comparing the WES hits

307 with the gene expression hits we identified 49 genes, while the CRISPRi/a and gene expression
308 studies had 76 genes in common (Fig. 4A). Three genes, *ATRAID, ATR,* and *ZBTB4* were
309 statistically significant in all three data types (Fig. 4A) (table S4). Focusing on *ATRAID*
310 specifically, we observed a ~50% decrease in *ATRAID* expression in the DTC and ONJ patients
311 where their gene expression had been measured. In exome sequencing on the AFF and ONJ
312 patients, interestingly, in *ATRAID* we detected two rare variants – hereafter referred to as the
313 'D5G/G32R variant' – that were present together in 3 out of 35 AFF and ONJ patients (2 out of
314 27 AFF; 1 out of 8 ONJ) (Fig. 4B).
315
316 We sought to determine the functional significance of decreased *ATRAID* mRNA expression
317 and the *ATRAID* D5G/G32R variant, both of which are associated with bad outcomes of N-BP
318 treatment (Fig. 4, A and B). To test the former, we introduced sub-endogenous levels of
319 *ATRAID* mRNA in *ATRAID* deficient cells such that the levels were similar to the reduced levels
320 seen in patients that experienced ONJ or DTC (~50% compared to wild-type controls) (Fig. 4C).
321 We refer to these *ATRAID* partially restored cells as '$ATRAID_{\text{low expr.}}$'. *ATRAID* deficient cells
322 conferred resistance to alendronate as expected, on the other hand, $ATRAID_{\text{low expr.}}$ cells were
323 hypersensitized to alendronate (Fig. 4D). Similarly, the *ATRAID* D5G/G32R variant, which we
324 identified in both the AFF and ONJ patients, conferred hypersensitivity to alendronate compared
325 with wild-type *ATRAID* (Fig. 4, E and F). Taken together, this suggests that bad patient
326 outcomes might reflect cellular hyper-response to N-BPs. In total, these findings support the
327 importance of ATRAID in bisphosphonate responsiveness in humans.
328
329 **DISCUSSION**
330 This work has focused on the physiological impact of *ATRAID* as a novel positive regulator
331 genetically upstream of *FDPS*. Here we use prenylation as an output of FDPS function.
332 Recently, we linked *FDPS* to DNA synthesis and damage (*46*). Considering that each of the

333 three top genes from the patient analysis, *ATRAID*, *ATR,* and *ZBTB4* (Fig. 4A)*,* are involved in
334 p53 responses – a well-known mediator of DNA damage (*47-50*) – it will be interesting to
335 determine whether these genes mediate their effects on p53 signaling via *FDPS*. The molecular
336 effects of N-BPs on FDPS require the novel transporter, SLC37A3 (*19*). Interestingly, the
337 SLC37A family member (*51*), *SLC37A2*, is mutated in dogs and gives rise to a bone overgrowth
338 phenotype that resembles the human disease, Caffey syndrome (*52, 53*). This phenotype is
339 particularly interesting because it suggests that natural ligands or drugs that inhibit the SLC37A
340 family might phenocopy N-BP treatment in increasing bone density. ATRAID binds NELL-1, a
341 secreted protein that promotes bone mineralization in mice and potentiates osteoblast
342 differentiation in an *ATRAID*-dependent manner (*54, 55*). It is also notable that NELL-1 is in pre-
343 clinical testing for the treatment of osteoporosis (*56*). In future studies, it will be interesting to
344 determine whether NELL-1 affects the responses to N-BPs we observe upon manipulating
345 *ATRAID*. There are rare, but serious clinical issues with N-BPs. Therefore, identifying those
346 patients who might experience these consequences when taking N-BPs is of paramount
347 importance. Perhaps utilizing *ATRAID* and/or other factors characterized herein as biomarker(s)
348 might eventually be such a diagnostic strategy.
349

350 **Materials and Methods**

351 ***Materials.*** Reagents were obtained from the following sources: antibodies to Rap1a (SC-1482)
352 from Santa Cruz Biotechnology; anti-HDJ-2/DNAJ Ab-1, Clone: KA2A5.6 (cat.# MS-225-P0),
353 anti-V5 (cat.# R960-25), and GAPDH (14C10) Rabbit mAb (cat.# 2118S) from Fisher Scientific;
354 rabbit polyclonal and monoclonal antibodies to PARP (cat.# 9532) from Cell Signaling
355 Technology; FuGENE 6 (cat.# E2691) and Complete Protease Cocktail (cat.# 11836170001)
356 from Roche; alendronate (cat.# 1012780-200MG), etidronate (cat.# P5248-10MG), tiludronate
357 (cat.# T4580-50MG), Acid Phosphatase Leukocyte (TRAP) kit (cat.# 387A-1KT), SYBR Green

358 JumpStart Taq ReadyMix (cat.# 4309155), calcein (cat.# C0875-5G), FLAG M2 affinity agarose
359 beads (Cat.# M2220), and anti-FLAG antibody (F3165), 3X FLAG peptide (F4799), ß-
360 glycerophosphate (cat.# 50020), ascorbic acid (cat.# A5960), RANKL (cat.# R0525), M-CSF
361 (cat.# M9170), dexamethasone (cat.# D4902), vitamin D3 (cat.# D1530), and alizarin red (cat.#
362 A3882-1G) from Sigma-Aldrich. Zoledronic acid (zoledronate, cat.# M 1875) from Moravek;
363 IMDM Glutamax, α-MEM, RPMI, SuperScript II Reverse Transcriptase, Platinum Pfx, Platinum
364 Taq DNA Polymerase and inactivated fetal calf serum (IFS) from Invitrogen; NEBNext Ultra II
365 Q5 Master Mix (cat.# M0544L), Sal I-HF (cat.# R3138L), Not I-HF (cat.# R3189L), BstXI (cat.#
366 R0113L), Blp I (cat.# R0585L) from New England Biolabs; NucleoSpin Blood DNA isolation kit
367 (cat.# 740950.50) from Macherey Nagel.
368
369 ***Cell lines and cell culture.*** KBM7 cell lines were cultured in IMDM with 10% IFS. K562 cell
370 lines were cultured in IMDM or RPMI with 10mM Glutamine with 10% FBS. HEK-293T cells
371 were cultured in DMEM with 10% FBS. RAW264.7 and primary mouse cells were cultured as
372 described below.
373
374 ***Haploid genetic screening.*** The genetic selection with alendronate was performed on 100
375 million mutagenized KBM7 cells (*57*). Cells were exposed to 165 μM alendronate and allowed to
376 recover for 4 weeks before harvesting the surviving cells and isolating genomic DNA. Analysis
377 of the screen was performed essentially as described previously (*57*). In brief, the sequences
378 flanking retroviral insertion sites were determined using inverse PCR followed by Illumina
379 sequencing. After mapping these sequences to the human genome, we counted the number of
380 inactivating mutations (i.e., mutations in the sense orientation or present in exon) per individual
381 Refseq-annotated gene as well as the total number of inactivating insertions for all Refseq-
382 annotated genes. For each gene, statistical enrichment was calculated by comparing how often
383 that gene was mutated in the drug-treated population with how often the gene carries an

384 insertion in the untreated control dataset. For each gene, the P-value (corrected for false
385 discovery rate) was calculated using the one-sided Fisher exact test (table S1).
386
387 ***CRISPRi/a genetic screening.*** We sought to improve the gene coverage in the zolendronate
388 CRISPRi screen we previously reported because we observed it was relatively under-sampled
389 compared to other CRISPRi/a screens we and others had performed (*19, 58*). We isolated
390 genomic DNA from biological replicate samples from our zolendronate screen and adapted the
391 Weissman lab library preparation protocol (*59*) with the following two changes to achieve
392 greater sgRNA coverage: 1) we increased the input genomic DNA from 0.5µg to 10µg of per
393 PCR reaction; and 2) we switched from Phusion to NEBNext Ultra II Q5 PCR enzyme.
394 Preparing the library with these modifications didn't change the top hits but it resulted in greater
395 number of sgRNAs for each gene being detected and more robust overlap of the gene scores
396 with our other CRISPRi/a screens with N-BPs.
397
398 ***cDNA manipulations and mutagenesis.*** The cDNAs for *ATRAID* were cloned from a human
399 R4 cell line cDNA library. For expression studies, all cDNAs were amplified by PCR and the
400 products were subcloned into the Sal 1 and Not 1 sites of pRK5 or pMSCV (*60*). The controls,
401 *metap2* and *tubulin*, were previously described (*61*). All constructs were verified by DNA
402 sequencing. To generate the 293T *ATRAID_KO* expressing *ATRAID-FLAG*, using Gibson
403 assembly we cloned the cDNA encoding *ATRAID* with a C-terminal Flag tag into a homologous
404 recombination vector targeting the *AAVS1* locus, with a GGGGSGGGGS flexible linker
405 (sequence: GGT GGA GGG GGA AGT GGC GGA GGA GGT TCA) added between the CDS
406 and the Flag tag. We transfected this vector along with pX330 expressing an sgRNA targeting
407 the *AAVS1* locus. To generate the *ATRAID* low expressing cell line (293T *ATRAID_KO* +
408 $ATRAID_{low\ expr}$), we used the same procedure, but cloned the cDNA encoding *ATRAID* with a C-
409 terminal V5 tag driven by a PGK promoter. Low expression was verified with multiple *ATRAID*

410 expression primers, described below. Mutagenesis to engineer *ATRAID* patient variants was
411 performed with a QuikChange site-directed mutagenesis kit (Agilent) following the
412 manufacturer's protocol. The viral vector, pLenti PGK hygromycin *ATRAID*-V5, used for
413 mutagenesis was previously described (*19*) and is based on Addgene clone ID: 19066.
414
415 ***sgRNA manipulations.*** Genome editing experiments were designed based on an established
416 protocol (*62*). In brief, the sgRNAs for *ATRAID* were cloned using Golden Gate assembly into
417 pSpCas9-BB-2A-GFP (PX438), a kind gift from Feng Zhang (Addgene #48138). All constructs
418 were verified by PCR and DNA sequencing. For the human *ATRAID* locus, one sgRNA targeting
419 exon 3 and another targeting exon 5 were used to act simultaneously and remove part of exon 3,
420 the entire exon 4 and part of exon 5.
421
422 Human *ATRAID*:
423 exon3 sgRNA_1: GCCTGATGAAAGTTTGGACC
424 exon3 sgRNA_2: CCCTGGTCCAAACTTTCATC
425 exon5 sgRNA_1: GTCCTGGAGGAATTAATGCC
426 exon5 sgRNA_2: GTCCTGGAGGAATTAATGCC
427
428 Mouse *ATRAID*:
429 GGATACATCGAAGCTAATGC
430 For generating *ATRAID* knockouts in RAW 264.7 cells, cells were transfected with PX438
431 carrying the above sgRNA. Mutation was confirmed by PCR and sequencing.
432
433 ***Cell viability assays.*** Wild-type or mutant cells were seeded at 20,000 cells per well in a 96-
434 well tissue culture plate and treated with indicated concentrations of compound or left untreated.
435 48 or 72 hours after treatment the cell viability was measured using a Cell-titer Glo colorimetric

436 assay (Promega) according to manufacturer's protocol. Viability is plotted as percentage viability
437 compared to untreated control.
438
439 For assays of apoptosis, cells were plated in 6-well dishes and exposed to alendronate for 48
440 hours. AnnexinV positive cells were quantified using flow cytometry with the Dead Cell
441 Apoptosis Kit with AnnexinV Alexa Fluor (488) and PI (Thermo Fisher Scientific #V13241)
442 following the manufacturer's instructions.
443
444 ***Protein analysis.*** All cells unless otherwise stated were rinsed twice with ice-cold PBS and
445 lysed with Triton-X 100 or NP-40 containing lysis buffer (40 mM HEPES [pH 7.4], 2 mM EDTA,
446 150 mM NaCl, 50 mM NaF, 1% Triton-X 100 or 1% NP-40, and one tablet of EDTA-free
447 protease inhibitors [Roche] per 25 ml or Halt protease-phosphatase inhibitor
448 (#78442 ThermoFisher Scientific)). Lysate is incubated at 4 centigrade for 15-30min with
449 constant inversion. The soluble fractions of cell lysates were isolated by centrifugation at 13,000
450 rpm for 10 min in a microcentrifuge. Lysate protein concentrations were normalized by Bradford
451 assay (Bio-Rad). Proteins were then denatured by the addition of sample buffer and by boiling
452 for 5 minutes, resolved using 4%-20% or 6% (for HDJ-2) SDS-PAGE (Invitrogen), and analyzed
453 by immunoblotting for the indicated proteins. Immunoblotting was performed as follows:
454 nitrocellulose membranes were blocked at room temperature (RT) with 5% non-fat milk for
455 45min. Membranes were then incubated overnight at 4°C with desired primary antibodies
456 dissolved in 5% milk. Membranes were then washed 3 times in TBST, each wash lasting 5min.
457 Membranes were then incubated at RT with desired secondary antibodies at 1:2000 in 5% milk
458 for 45min. HRP-conjugated or fluorescent secondary antibodies (Santa Cruz Biotechnology or
459 Thermo Fisher, respectively) were used for detection. Membranes were then washed 3 times in
460 TBST, each wash lasting 5min. Signal from membranes using HRP-conjugated secondary
461 antibodies were captured using a camera and those using fluorescent secondary antibodies

462 were imaged on a GE Typhoon Trio imager. The small GTPase Rap1A protein prenylation can
463 be detected by Western blot analysis using an antibody that specifically binds to its
464 unprenylated form (*63, 64*) (Santa Cruz, SC-1482).
465
466 ***RAW 264.7 differentiation*.** RAW 264.7 cells were maintained in DMEM + 10% FBS + 1X
467 penicillin/streptomycin. Differentiation of RAW cells to osteoclasts was achieved following the
468 protocol of Collin-Osdoby et al. (*42*) where cells were treated with 35ng/ml RANKL (R&D
469 Systems) for 6 days. For experiments with alendronate, the drug was added at the indicated
470 concentrations 48 hours prior to collection.
471
472 ***Primary bone marrow isolation and osteoclast differentiation.*** Primary bone marrow was
473 isolated from the femurs, tibiae, and spine of wildtype and *ATRAID*^{KO} mice, enriched to
474 macrophages and differentiated to osteoclasts following the protocol of Tevlin et al. (*41*). Where
475 indicated, cells were treated with the indicated concentrations of alendronate 48 hours before
476 collection. Note: alendronate responsiveness can differ between different osteoclast cell
477 contexts (*65*). In our hands, isolated primary osteoclasts were more sensitive to alendronate
478 than the RAW 264.7 cell line. Therefore, we used higher doses of alendronate with RAW 264.7
479 cells vs. isolated primary cells (30μM and 80μM vs. 10μM and 30μM).
480
481 ***Co-culture of primary osteoblasts and osteoclasts.*** Murine bone marrow macrophages and
482 bone marrow stromal cells were isolated from the long bones of wild-type and *ATRAID* deficient
483 mice. Murine bone marrow macrophages were differentiated to osteoclasts using M-CSF and
484 RANKL in α-MEM + 10% FBS. Murine bone marrow stromal cells were differentiated to
485 osteoblasts using ß-glycerophosphate and ascorbic acid in α-MEM + 20% FBS. 200,000
486 osteoblasts and 300,000 osteoclasts were co-cultured in six-well dishes in α-MEM + 10% FBS
487 10nM 1,25$(OH)_2$ vitamin D3, and 100nM dexamethasone and treated with the indicated

488 concentrations of alendronate for 96 hours followed by tartrate acid phosphatase assay
489 following the manufacturer's protocol. Images of the 6-well dishes were captured by camera and
490 the total TRAP staining on these images was quantified using ImageJ software using the
491 Analyze->Analyze Particle workflow.

492 ***Gene expression analysis.*** Total RNA was isolated and reverse-transcription was performed
493 from cells or tissues in the indicated conditions. The resulting cDNA was diluted in Dnase-free
494 water (1:20) followed by quantification by real-time PCR. mRNA transcript levels were measured
495 using Applied Biosystems 7900HT Sequence Detection System v2.3 software. All Data are
496 expressed as the ratio between the expression of target gene to the housekeeping genes 36B4
497 and/or GAPDH. Each treated sample was normalized to the level of the controls in the same cell
498 type.
499
500 Human Primer sequences (for clarity, denoted with prefix: "h" for human):
501 hATRAID exon1-F' – GGATGGAGGGGCCCGAGTTTCTG
502 hATRAID exon2-R' – CCCAAGATGGTGCCCTTCTGATTC
503
504 hATRAID exon6-F' – CCATGGATACAAGTGTATGCGCC
505 hATRAID exon 7-R' – TCATGAAGTCTTGGCTTTTCGGC
506
507 hRPLP0-F'- CAGATTGGCTACCCAACTGTT
508 hRPLP0-R'- GGAAGGTGTAATCCGTCTCCAC
509
510 hTBP-F'- GAGCCAAGAGTGAAGAACAGTC
511 hTBP-R'- GCTCCCCACCATATTCTGAATCT
512

513

514 Mouse Primer sequences (for clarity, denoted with prefix: “m” for mouse):

515 mATRAID exon3-F’ – GATCTTCAGAACTGTTCCCTGAAG

516 mATRAID exon4-R’ – GCTGAGTAAACCCACGGAAGGTG

517

518 mATRAID exon5-F’ – CTTCTTTCAAGGACAAGCAGATTTG

519 mATRAID exon 7-R’ – GAATCCCAAAGAACATAAGCAGTG

520

521 mACTB- F’- TGTCGAGTCGCGTCCA

522 mACTB- R’ – ATGCCGGAGCCGTTGTC

523

524 mRPLP0- F’ – TGCTCGACATCACAGAGCAG

525 mRPLP0- R’ – ACGCGCTTGTACCCATTGAT

526

527 mRANK – F’ – GCAGCTCAACAAGGATACGG

528 mRANK – R’- TAGCTTTCCAAGGAGGGTGC

529

530 mTRAP –F’ – AAGAGATCGCCAGAACCGTG

531 mTRAP – R’ – CGTCCTCAAAGGTCTCCTGG

532

533 mCTSK – F’ – CCTTCCAATACGTGCAGCAG

534 mCTSK- R’ – CATTTAGCTGCCTTTGCCGT

535

536 ***Generation and genotyping of ATRAID KO mice****.* Chimeric mice were obtained by

537 microinjection of the correctly targeted *ATRAID* EUCOMM ES clones (HEPD0577_2_D01 and

538 HEPD0577_2_E01) (*66, 67*) into BALB/C blastocysts and crossed with C57BL/6 mice to obtain

539 offspring with germline transmission. Heterozygous mice for the floxed *ATRAID* allele
540 (*ATRAID*$^{loxP/+}$), were crossed to C57BL/6 mice expressing the Cre-recombinase transgene from
541 the full-body CMV promoter (*68*). Mice analyzed in this study were 100% C57BL/6.
542
543 All experiments involving mice were performed with protocols approved by the Harvard and
544 Washington University Animal Studies Committees. We confirm that we have complied with all
545 relevant ethical regulations. All mice were housed under a 12-hour light cycle and fed standard
546 chow diet ad libitum.
547
548 PCR genotyping of all WT and *ATRAID* deficient mice were performed with primers that detect
549 the following:
550 4) This generates a 140bp product and indicates the presence of the transgene.
551 Transgene (92 upstream) F' CAGCCATATCACATCTGTAGAG
552 Transgene (92 upstream) R' GAGTTTGGACAAACCACAACTAG
553 2) This indicates recombination and is detectable in mice also expressing CRE
554 Del F' CTGCATTCTAGTTGTGGTTTGTCC
555 Del R' CAGGAGGTAGTGCAAGCCTTTG
556 3) Wild-type *ATRAID* primers spanning *ATRAID* exons 3 and 4. This PCR product is not
557 detectable in homozygous null animals.
558 Exon ¾ F' CAGAACTGTTCCCTGAAGGATCCTGGTC
559 Exon ¾ R' GTACACACTGTTAGCGCTCTGTTTGC
560 4) These generic CRE primers give a ~100bp product indicates the presence of the CRE
561 transgene.
562 CRE F' GCG GTC TGG CAG TAA AAA CTA TC
563 CRE R' GTG AAA CAG CAT TGC TGT CAC TT
564

565 ***Serum ELISA assays.*** Cardiac puncture blood of mice of the indicated ages was obtained and
566 centrifuged at low speed at 4°C for 15 min, and serum was isolated. Gla-Osteocalcin (Mouse
567 Gla-Osteocalcin High Sensitive EIA Kit from Clontech, cat.# MK127) and C-terminus cross-
568 linked telopeptides of type I collagen CTX-I (RatLaps EIA Kit from Immunodiagnosticsystems
569 Inc., Bolden, UK, AC-06F1) were quantified following the manufacturer instructions.
570
571 ***Animal procedures***. Age and sex matched mice were randomly assigned to treatment groups
572 within each genotype. For the basal characterization of WT and *ATRAID* deficient mice and for
573 the OVX experiments the mice were litter-matched. For the senile osteoporosis experiments the
574 animals were originally derived from the same litter but were bred as cohorts. All animal
575 experiments were replicated two to four times spanning independent days to ensure
576 reproducibility. No outlier animals were excluded from any downstream analysis.
577
578 Ovariectomy or sham operations were performed on 3.5-month-old females as detailed
579 previously (*69*). Briefly, the ovaries were exposed through an abdominal approach and either
580 resected after clipping the blood vessels or left in place (sham operation). The muscle and skin
581 of the abdomen were sutured. Mice were given an intraperitoneal injection of buprenex
582 immediately after surgery and then every twelve hours for 48 hours post-surgery. Immediately
583 preceding OVX, vehicle (phosphate buffered saline) or 100 µg/kg alendronate (both provided by
584 Sigma) was injected intra-peritoneally every week for 4 weeks. These doses were chosen
585 based on the anti-resorptive activity of alendronate in different species (*70, 71*).
586
587 ***Bone microstructure.*** A high-resolution desktop micro-tomographic imaging system (µCT40,
588 Scanco Medical AG, Bruttisellen, Switzerland) was used to assess cortical and trabecular bone
589 microarchitecture and morphology in the femoral mid-diaphysis and distal metaphysis,
590 respectively. Scans were acquired using a 10 μm^3 isotropic voxel size, 70 kVP peak x-ray tube

591 potential, 114 mAs x-ray intensity, 200 ms integration time, and were subjected to Gaussian
592 filtration and segmentation. Regions of interest (ROIs) were selected 50 slices above and below
593 the femoral longitudinal midpoint or 100 slices above the growth plate of the distal femur to
594 evaluate the cortical and trabecular compartment, respectively. Image acquisition and analysis
595 adhered to the JBMR guidelines for the use of μCT for the assessment of bone
596 microarchitecture in rodents (*31*). To judge the effect sizes in our μCT experiments, it is notable
597 that both OVX and ALN influenced μCT parameters in wild-type mice of a magnitude in our
598 hands (~10-20%) that is highly consistent with what has been previously shown in the strain we
599 used, C57BL/6 (*39, 72*).
600
601 ***Bone biomechanics.*** Mechanical testing in a 3-point bending to failure was conducted on
602 femora after μCT. Briefly, hydrated femora were stabilized over supports 7mm apart and a
603 loading force was applied in the anteroposterior direction midway between the supports (Instron,
604 Norwood, MA, USA). Test curves were analyzed to determine ultimate force to failure and
605 stiffness as described previously (*32, 73*).
606
607 ***Bone histomorphometry.*** To label mineralizing fronts, mice were injected intraperitoneally with
608 calcein (15 mg/kg i.p., Sigma-Aldrich) and alizarin red (30 mg/kg; Sigma) were intraperitoneally
609 injected 7 and 2 days, respectively, before euthanasia. Bone was fixed in 10% (vol/vol) neutral
610 buffered formalin for 24 h, processed through a series of graded alcohols, and decalcified.
611 Decalcified vertebrae or femurs were embedded in paraffin and 2-4 h, processed through a
612 series of graded alcohols, and Tartrate resistant acid phosphatase (TRAP) stain was performed.
613 Undecalcified femora were embedded in methyl methacrylate and the whole bone were cut and
614 stained for TRAP or analyzed for calcein and alizarin red fluorescence. Quantitative
615 histomorphometry was performed using a commercial software (OSTEO II, Bioquant, Nashville,

616 TN, USA), and standard parameters of bone remodeling were determined as detailed elsewhere
617 (*74*).
618
619 ***Statistics analysis.*** Unless otherwise specified, group means were compared by one-tailed
620 Student t-test for unpaired samples. Data on repeated measures were analyzed by ANOVA,
621 followed by a post-hoc multiple Holm–Sidak method t-test. All data are expressed as the mean
622 ± s.d with numbers of samples indicated in figure legends. *P* values are indicated in each figure
623 legend, and values less than 0.05 were considered significant. All code used to generate
624 statistics and correlations for this project can be found at https://github.com/tim-
625 peterson/ATRAID.
626
627 ***Transcriptional profiling analysis.*** The multiple myeloma, osteonecrosis of the jaw (ONJ)
628 microarray gene expression was performed as previously described (*43*) using the Affymetrix
629 U133 Plus 2.0 array platform (Affymetrix, Santa Clara, CA, USA) on total RNA isolated from
630 peripheral blood mononuclear cells (GEO accession #: GSE7116). 21 multiple myeloma
631 patients with a history of N-BP use were included in the study. 11 patients (52.4%) reported to
632 have ONJ. The breast cancer bone marrow micrometastases (a.k.a., DTC) microarray gene
633 expression data was generated as previously described (*44*) and also used the Affymetrix U133
634 Plus 2.0 array platform. DTC profiling was performed on tumor biopsies of 81 patients (GEO
635 accession #: GSE71258). 54 breast cancer patients treated with zometa (zoledronate) were
636 included in the study. N-BPs directly inhibit tumor growth and angiogenesis (*75, 76*). 14 patients
637 (25.9%) eventually died and 40 patients (74.1%) survived. Her-2 negative patients were divided
638 into two categories following randomization to the zoledronate arm: those that who had DTC
639 reoccurrences or lived less than 1000 days and those who lived at least 2500 days.
640

641 Quantile normalization was used for all differential expression analysis, and all the normalization
642 procedures were performed using function normalizeQuantiles in the R Bioconductor package
643 limma (*77*). Gene expression data was filtered using function filterfun in the R Bioconductor
644 package genefilter (*78*). Probes with expression values over 5 in less than 25% of the samples
645 were removed. Comparison between groups were estimated using an empirical Bayes method
646 (*79*), and variances across all genes were used to estimate the variance of each gene. Raw p-
647 values were calculated from a moderate t-test, and false discovery rate (FDR) adjusted p-values
648 were obtained based on Benjamini and Hochberg's methods for multiple testing. Log_2 fold
649 changes between the experimental conditions were calculated for each gene as well.
650
651 Affy probe IDs were transformed into gene symbols based on the R Bioconductor package,
652 hgu133plus2.db (*80*). In Fig. 4A, differentially regulated genes for the -/+ONJ patients were
653 identified by having adjusted p-values smaller than 0.05, while potential differentially-regulated
654 genes for the <1000 vs. >2500 days with breast cancer patients with disseminated tumor cells
655 (DTC) were identified by having raw p-value smaller than 0.05. For the ONJ dataset, 1992
656 genes were significant. For the DTC dataset, 1854 genes were significant.
657
658 ***Exome sequencing analysis.*** Exome sequencing data was generated from blood leukocyte
659 DNA for 27 bisphosphonate treated osteoporosis cases with atypical femoral fractures (AFF), 11
660 bisphosphonate treated osteoporosis cases without atypical femoral fractures, and 8
661 bisphosphonate multiple myeloma or breast cancer cases with osteonecrosis of the jaw (ONJ).
662 Exome capture was performed using Agilent All-exome capture kits. Sequencing was performed
663 using paired-end Illumina sequencing. Analysis of exome sequencing data was performed in-
664 house using our previously described methods (*81, 82*). Briefly, FASTQ formatted sequences
665 were aligned to the hg37 human reference sequence (NCBI GRCh37) using BWA (*83*).
666 Mapped reads were filtered to remove duplicate reads with the same paired start sites. The

667 Binary sequence Alignment/Map (BAM) formatted alignments were then processed using the
668 Genome Analysis Toolkit (GATK) Haplotype Caller (*84, 85*) and genotypes jointly called
669 together with all in-house control exome sequenced individuals. Variants were filtered for read-
670 depth (>8x), genotype quality (GQ>20), and GATK-calculated variant quality score recalibration
671 (VQSR). Allele frequencies were annotated using the gnomAD database (*86*). Variant positions
672 were processed excluding those with call rates <0.95 or Hardy-Weinberg equilibrium P-values <
673 10^{-5}. Variants were annotated using Seattleseq:
674 http://snp.gs.washington.edu/SeattleSeqAnnotation151/. Genes with multiple variants with non-
675 Finnish European (NFE) allele frequencies less than 0.05 only in cases were considered. From
676 dbSNP, https://www.ncbi.nlm.nih.gov/SNP/ : For the *ATRAID* gene, the D5G variant is found on
677 chromosome 2 position: 27212382 – rs1275533. The G32R variant is found on chromosome 2
678 position: 27212297 – rs11556163.
679
680 The ethnic breakdown of the AFF cases is: 25/27 European American (EA), 3/27 Asian
681 American (AA), 0/27 African American. The ethnic breakdown of the controls is 8/11 European
682 American and 3/11 unknown. For *ATRAID*, the D5G variant is present in 2 out of 27 AFF
683 patients. Though this allele wasn't detected in the 11 control samples, it is present in a
684 population of European Americans (EA) that is representative of the study population at a
685 prevalence of 0.0139 and in Asian Americans (AA) at a prevalence of 0.002. Therefore, the
686 D5G allele is (2/27) / (0.0139 * 25/27 + 0.002 * 3/27) = 5.66X enriched in cases compared to a
687 representative population to that of the cases. For the G32R *ATRAID* allele the enrichment is:
688 (2/27) / (0.0149 * 25/27 + 0.002 * 3/27) = 5.28. Because we have incomplete information on the
689 ONJ cases, we used the EA frequency for our enrichment calculations: the D5G allele is (1/8) /
690 (0.0139 * 8/8) = 7.19X enriched in cases compared to a representative population. For the
691 G32R allele the enrichment is: (1/8) / (0.0149 * 8/8) = 6.71X. A simple binomial test,
692 binom.test(), was used to calculate the p-value for each *ATRAID* variant in AFF and ONJ cases.

693 For the D5G allele, p-value = 0.01262 – binom.test(3, 35, 0.0139). For the G32R, p-value =
694 0.01518 – binom.test(3, 35, 0.0149).
695
696 ***Functional validation of ATRAID patient alleles.*** For testing the effects of reduced *ATRAID*
697 expression**,** *ATRAID* deficient HEK-293T cells were stably infected with sub-endogenous levels
698 of variant "v3" of wild-type *ATRAID*. These cells were then compared with wild-type HEK-293T
699 and the parent *ATRAID* deficient line in cell viability assays. For the rs1275533 variant, the
700 amino acid change, D5G, corresponds to the v3 ATRAID amino acid sequence and the same
701 variant is D60G on the longer, v2 *ATRAID* isoform. For the rs11556163 variant, G32R is only
702 present on v2 *ATRAID*. Both *ATRAID* variants were found together in each AFF or ONJ case
703 identified, which suggested these variants are linked. Thus, to recapitulate the patient
704 genotypes, we therefore introduced both v2 and v3 wild-type or variant forms of ATRAID in
705 *ATRAID* deficient cells. This means there were three differences between the wild-type and
706 ATRAID D5G/G32R variant cell lines we generated – two variants on v2 ATRAID and one
707 variant on v3 ATRAID.
708
709 **Supplementary Materials**
710 **Fig. S1, related to Fig. 1. ATRAID is required for molecular responses to N-BPs.**
711 **Fig. S2, related to Fig. 2. ATRAID is required for organismal responses to N-BPs.**
712 **Fig. S3, related to Fig. 3. ATRAID is required cell-autonomously for N-BP inhibition of**
713 **osteoclast function.**
714 **Table S1, related to Fig. 1 and fig. S1. Haploid genomic screen raw data for alendronate.**
715 **Table S2, related to Fig. 2 and fig. S2. Statistics for animal studies.**
716 **Table S3, related to Fig. 3 and fig. S3. Statistics for animal and co-culture studies.**
717 **Table S4, related to Fig. 4. Gene expression, sequencing, and growth phenotype data for**
718 **ONJ, DTC, AFF, and CRISPRi and CRISPRa studies.**

References and Notes:

1. J. J. Carey, L. Palomo, Bisphosphonates and osteonecrosis of the jaw: innocent association or significant risk? *Cleveland Clinic journal of medicine* **75**, 871-879 (2008).
2. J. P. van den Bergh, T. A. van Geel, P. P. Geusens, Osteoporosis, frailty and fracture: implications for case finding and therapy. *Nat Rev Rheumatol* **8**, 163-172 (2012).
3. R. E. Coleman, E. V. McCloskey, Bisphosphonates in oncology. *Bone* **49**, 71-76 (2011).
4. D. M. Black, C. J. Rosen, Clinical Practice. Postmenopausal Osteoporosis. *N Engl J Med* **374**, 254-262 (2016).
5. N. B. Watts, D. L. Diab, Long-term use of bisphosphonates in osteoporosis. *J Clin Endocrinol Metab* **95**, 1555-1565 (2010).
6. Y. Bi, Y. Gao, D. Ehirchiou, C. Cao, T. Kikuiri, A. Le, S. Shi, L. Zhang, Bisphosphonates cause osteonecrosis of the jaw-like disease in mice. *Am J Pathol* **177**, 280-290 (2010).
7. S. Khosla, J. A. Cauley, J. Compston, D. P. Kiel, C. Rosen, K. G. Saag, E. Shane, Addressing the Crisis in the Treatment of Osteoporosis: A Path Forward. *J Bone Miner Res*, (2016).
8. S. P. Luckman, D. E. Hughes, F. P. Coxon, R. Graham, G. Russell, M. J. Rogers, Nitrogen-containing bisphosphonates inhibit the mevalonate pathway and prevent post-translational prenylation of GTP-binding proteins, including Ras. *J Bone Miner Res* **13**, 581-589 (1998).
9. E. van Beek, E. Pieterman, L. Cohen, C. Lowik, S. Papapoulos, Nitrogen-containing bisphosphonates inhibit isopentenyl pyrophosphate isomerase/farnesyl pyrophosphate synthase activity with relative potencies corresponding to their antiresorptive potencies in vitro and in vivo. *Biochem Biophys Res Commun* **255**, 491-494 (1999).
10. J. D. Bergstrom, R. G. Bostedor, P. J. Masarachia, A. A. Reszka, G. Rodan, Alendronate is a specific, nanomolar inhibitor of farnesyl diphosphate synthase. *Arch Biochem Biophys* **373**, 231-241 (2000).
11. M. J. Favus, Bisphosphonates for osteoporosis. *N Engl J Med* **363**, 2027-2035 (2010).
12. C. J. Rosen, Clinical practice. Postmenopausal osteoporosis. *N Engl J Med* **353**, 595-603 (2005).
13. R. Coleman, The use of bisphosphonates in cancer treatment. *Ann N Y Acad Sci* **1218**, 3-14 (2011).
14. S. Jha, Z. Wang, N. Laucis, T. Bhattacharyya, Trends in Media Reports, Oral Bisphosphonate Prescriptions, and Hip Fractures 1996-2012: An Ecological Analysis. *J Bone Miner Res* **30**, 2179-2187 (2015).
15. A. A. Reszka, G. A. Rodan, Nitrogen-containing bisphosphonate mechanism of action. *Mini Rev Med Chem* **4**, 711-719 (2004).
16. V. Breuil, F. Cosman, L. Stein, W. Horbert, J. Nieves, V. Shen, R. Lindsay, D. W. Dempster, Human osteoclast formation and activity in vitro: effects of alendronate. *J Bone Miner Res* **13**, 1721-1729 (1998).
17. Z. Zimolo, G. Wesolowski, G. A. Rodan, Acid extrusion is induced by osteoclast attachment to bone. Inhibition by alendronate and calcitonin. *J Clin Invest* **96**, 2277-2283 (1995).
18. D. E. Hughes, K. R. Wright, H. L. Uy, A. Sasaki, T. Yoneda, G. D. Roodman, G. R. Mundy, B. F. Boyce, Bisphosphonates promote apoptosis in murine osteoclasts in vitro and in vivo. *J Bone Miner Res* **10**, 1478-1487 (1995).
19. Z. Yu, L. E. Surface, C. Y. Park, M. A. Horlbeck, G. A. Wyant, M. Abu-Remaileh, T. R. Peterson, D. M. Sabatini, J. S. Weissman, E. K. O'Shea, Identification of a transporter

complex responsible for the cytosolic entry of nitrogen-containing-bisphosphonates. *Elife* **7**, (2018).
20. J. E. Carette, C. P. Guimaraes, M. Varadarajan, A. S. Park, I. Wuethrich, A. Godarova, M. Kotecki, B. H. Cochran, E. Spooner, H. L. Ploegh, T. R. Brummelkamp, Haploid genetic screens in human cells identify host factors used by pathogens. *Science* **326**, 1231-1235 (2009).
21. A. J. Roelofs, K. Thompson, F. H. Ebetino, M. J. Rogers, F. P. Coxon, Bisphosphonates: molecular mechanisms of action and effects on bone cells, monocytes and macrophages. *Curr Pharm Des* **16**, 2950-2960 (2010).
22. F. Zhu, W. Yan, Z. L. Zhao, Y. B. Chai, F. Lu, Q. Wang, W. D. Peng, A. G. Yang, C. J. Wang, Improved PCR-based subtractive hybridization strategy for cloning differentially expressed genes. *Biotechniques* **29**, 310-313 (2000).
23. S. Bashiardes, R. Veile, M. Allen, C. A. Wise, M. Dobbs, J. A. Morcuende, L. Szappanos, J. A. Herring, A. M. Bowcock, M. Lovett, SNTG1, the gene encoding gamma1-syntrophin: a candidate gene for idiopathic scoliosis. *Hum Genet* **115**, 81-89 (2004).
24. Y. Z. Liu, S. G. Wilson, L. Wang, X. G. Liu, Y. F. Guo, J. Li, H. Yan, P. Deloukas, N. Soranzo, U. Chinappen-Horsley, A. Cervino, F. M. Williams, D. H. Xiong, Y. P. Zhang, T. B. Jin, S. Levy, C. J. Papasian, B. M. Drees, J. J. Hamilton, R. R. Recker, T. D. Spector, H. W. Deng, Identification of PLCL1 gene for hip bone size variation in females in a genome-wide association study. *PLoS One* **3**, e3160 (2008).
25. E. Shimizu, J. Tamasi, N. C. Partridge, Alendronate affects osteoblast functions by crosstalk through EphrinB1-EphB. *J Dent Res* **91**, 268-274 (2012).
26. G. Yang, F. Yu, H. Fu, F. Lu, B. Huang, L. Bai, Z. Zhao, L. Yao, Z. Lu, Identification of the distinct promoters for the two transcripts of apoptosis related protein 3 and their transcriptional regulation by NFAT and NFkappaB. *Mol Cell Biochem* **302**, 187-194 (2007).
27. Phyre2, http://www.sbg.bio.ic.ac.uk/phyre2/html/page.cgi?id=index. *Protein Homology/analogY Recognition Engine V 2.0*, (website).
28. R. G. Russell, Bisphosphonates: the first 40 years. *Bone* **49**, 2-19 (2011).
29. K. Thompson, M. J. Rogers, F. P. Coxon, J. C. Crockett, Cytosolic entry of bisphosphonate drugs requires acidification of vesicles after fluid-phase endocytosis. *Mol Pharmacol* **69**, 1624-1632 (2006).
30. W. C. Skarnes, B. Rosen, A. P. West, M. Koutsourakis, W. Bushell, V. Iyer, A. O. Mujica, M. Thomas, J. Harrow, T. Cox, D. Jackson, J. Severin, P. Biggs, J. Fu, M. Nefedov, P. J. de Jong, A. F. Stewart, A. Bradley, A conditional knockout resource for the genome-wide study of mouse gene function. *Nature* **474**, 337-342 (2011).
31. M. L. Bouxsein, S. K. Boyd, B. A. Christiansen, R. E. Guldberg, K. J. Jepsen, R. Muller, Guidelines for assessment of bone microstructure in rodents using micro-computed tomography. *J Bone Miner Res* **25**, 1468-1486 (2010).
32. http://www.musculoskeletalcore.wustl.edu/mm/files/Understanding%203pt%20Bending%20outcomes.pdf.
33. C. Rosenquist, C. Fledelius, S. Christgau, B. J. Pedersen, M. Bonde, P. Qvist, C. Christiansen, Serum CrossLaps One Step ELISA. First application of monoclonal antibodies for measurement in serum of bone-related degradation products from C-terminal telopeptides of type I collagen. *Clin Chem* **44**, 2281-2289 (1998).
34. D. W. Dempster, J. E. Compston, M. K. Drezner, F. H. Glorieux, J. A. Kanis, H. Malluche, P. J. Meunier, S. M. Ott, R. R. Recker, A. M. Parfitt, Standardized nomenclature, symbols, and units for bone histomorphometry: a 2012 update of the

817 report of the ASBMR Histomorphometry Nomenclature Committee. *J Bone Miner Res*
818 **28**, 2-17 (2013).
819 35. P. Ballanti, S. Minisola, M. T. Pacitti, L. Scarnecchia, R. Rosso, G. F. Mazzuoli, E.
820 Bonucci, Tartrate-resistant acid phosphate activity as osteoclastic marker: sensitivity of
821 cytochemical assessment and serum assay in comparison with standardized osteoclast
822 histomorphometry. *Osteoporos Int* **7**, 39-43 (1997).
823 36. X. Zou, J. Shen, F. Chen, K. Ting, Z. Zheng, S. Pang, J. N. Zara, J. S. Adams, C. Soo,
824 X. Zhang, NELL-1 binds to APR3 affecting human osteoblast proliferation and
825 differentiation. *FEBS Lett* **585**, 2410-2418 (2011).
826 37. M. Ferron, J. Wei, T. Yoshizawa, A. Del Fattore, R. A. DePinho, A. Teti, P. Ducy, G.
827 Karsenty, Insulin signaling in osteoblasts integrates bone remodeling and energy
828 metabolism. *Cell* **142**, 296-308 (2010).
829 38. H. A. Fleisch, Bisphosphonates: preclinical aspects and use in osteoporosis. *Ann Med*
830 **29**, 55-62 (1997).
831 39. M. P. Watkins, J. Y. Norris, S. K. Grimston, X. Zhang, R. J. Phipps, F. H. Ebetino, R.
832 Civitelli, Bisphosphonates improve trabecular bone mass and normalize cortical
833 thickness in ovariectomized, osteoblast connexin43 deficient mice. *Bone* **51**, 787-794
834 (2012).
835 40. K. Watanabe, A. Hishiya, Mouse models of senile osteoporosis. *Mol Aspects Med* **26**,
836 221-231 (2005).
837 41. R. Tevlin, A. McArdle, C. K. Chan, J. Pluvinage, G. G. Walmsley, T. Wearda, O.
838 Marecic, M. S. Hu, K. J. Paik, K. Senarath-Yapa, D. A. Atashroo, E. R. Zielins, D. C.
839 Wan, I. L. Weissman, M. T. Longaker, Osteoclast derivation from mouse bone marrow. *J*
840 *Vis Exp*, e52056 (2014).
841 42. P. Collin-Osdoby, P. Osdoby, RANKL-mediated osteoclast formation from murine RAW
842 264.7 cells. *Methods Mol Biol* **816**, 187-202 (2012).
843 43. N. Raje, S. B. Woo, K. Hande, J. T. Yap, P. G. Richardson, S. Vallet, N. Treister, T.
844 Hideshima, N. Sheehy, S. Chhetri, B. Connell, W. Xie, Y. T. Tai, A. Szot-Barnes, M.
845 Tian, R. L. Schlossman, E. Weller, N. C. Munshi, A. D. Van Den Abbeele, K. C.
846 Anderson, Clinical, radiographic, and biochemical characterization of multiple myeloma
847 patients with osteonecrosis of the jaw. *Clin Cancer Res* **14**, 2387-2395 (2008).
848 44. J. Xiang, M. A. Hurchla, F. Fontana, X. Su, S. R. Amend, A. K. Esser, G. J. Douglas, C.
849 Mudalagiriyappa, K. E. Luker, T. Pluard, F. O. Ademuyiwa, B. Romagnoli, G. Tuffin, E.
850 Chevalier, G. D. Luker, M. Bauer, J. Zimmermann, R. L. Aft, K. Dembowsky, K. N.
851 Weilbaecher, CXCR4 Protein Epitope Mimetic Antagonist POL5551 Disrupts Metastasis
852 and Enhances Chemotherapy Effect in Triple-Negative Breast Cancer. *Mol Cancer Ther*
853 **14**, 2473-2485 (2015).
854 45. J. L. Jiwoong Park, Sandeep Kumar, Damon T. Burrow, Nicholas L. Bean, Chris Chow,
855 Nicholas C. Jacobs, Niki Song, Sarah S. Diemar, Luke A. Gilbert, Timothy R. Peterson,
856 Using cell fitness to reduce human biases in human gene characterization. *in*
857 *preparation*, (2019).
858 46. M. A. Horlbeck, A. Xu, M. Wang, N. K. Bennett, C. Y. Park, D. Bogdanoff, B. Adamson,
859 E. D. Chow, M. Kampmann, T. R. Peterson, K. Nakamura, M. A. Fischbach, J. S.
860 Weissman, L. A. Gilbert, Mapping the Genetic Landscape of Human Cells. *Cell* **174**,
861 953-967 e922 (2018).
862 47. S. Han, Q. Lu, N. Wang, Apr3 accelerates the senescence of human retinal pigment
863 epithelial cells. *Mol Med Rep* **13**, 3121-3126 (2016).
864 48. E. Lecona, O. Fernandez-Capetillo, Targeting ATR in cancer. *Nat Rev Cancer*, (2018).
865 49. D. Yamada, R. Perez-Torrado, G. Filion, M. Caly, B. Jammart, V. Devignot, N. Sasai, P.
866 Ravassard, J. Mallet, X. Sastre-Garau, M. L. Schmitz, P. A. Defossez, The human

867 protein kinase HIPK2 phosphorylates and downregulates the methyl-binding
868 transcription factor ZBTB4. *Oncogene* **28**, 2535-2544 (2009).
869 50. A. Weber, J. Marquardt, D. Elzi, N. Forster, S. Starke, A. Glaum, D. Yamada, P. A.
870 Defossez, J. Delrow, R. N. Eisenman, H. Christiansen, M. Eilers, Zbtb4 represses
871 transcription of P21CIP1 and controls the cellular response to p53 activation. *EMBO J*
872 **27**, 1563-1574 (2008).
873 51. J. Y. Chou, B. C. Mansfield, The SLC37 family of sugar-phosphate/phosphate
874 exchangers. *Curr Top Membr* **73**, 357-382 (2014).
875 52. M. K. Hytonen, M. Arumilli, A. K. Lappalainen, M. Owczarek-Lipska, V. Jagannathan, S.
876 Hundi, E. Salmela, P. Venta, E. Sarkiala, T. Jokinen, D. Gorgas, J. Kere, P. Nieminen,
877 C. Drogemuller, H. Lohi, Molecular Characterization of Three Canine Models of Human
878 Rare Bone Diseases: Caffey, van den Ende-Gupta, and Raine Syndromes. *PLoS Genet*
879 **12**, e1006037 (2016).
880 53. A. Guerin, L. Dupuis, R. Mendoza-Londono, in *GeneReviews((R)),* M. P. Adam, H. H.
881 Ardinger, R. A. Pagon, S. E. Wallace, L. J. H. Bean, K. Stephens, A. Amemiya, Eds.
882 (Seattle (WA), 1993).
883 54. X. Zou, J. Shen, F. Chen, K. Ting, Z. Zheng, S. Pang, J. N. Zara, J. S. Adams, C. Soo,
884 X. Zhang, NELL-1 binds to APR3 affecting human osteoblast proliferation and
885 differentiation. *FEBS Lett* **585**, 2410-2418 (2011).
886 55. J. Desai, M. E. Shannon, M. D. Johnson, D. W. Ruff, L. A. Hughes, M. K. Kerley, D. A.
887 Carpenter, D. K. Johnson, E. M. Rinchik, C. T. Culiat, Nell1-deficient mice have reduced
888 expression of extracellular matrix proteins causing cranial and vertebral defects. *Hum*
889 *Mol Genet* **15**, 1329-1341 (2006).
890 56. A. W. James, J. Shen, X. Zhang, G. Asatrian, R. Goyal, J. H. Kwak, L. Jiang, B. Bengs,
891 C. T. Culiat, A. S. Turner, H. B. Seim Iii, B. M. Wu, K. Lyons, J. S. Adams, K. Ting, C.
892 Soo, NELL-1 in the treatment of osteoporotic bone loss. *Nat Commun* **6**, 7362 (2015).
893 57. J. E. Carette, C. P. Guimaraes, I. Wuethrich, V. A. Blomen, M. Varadarajan, C. Sun, G.
894 Bell, B. Yuan, M. K. Muellner, S. M. Nijman, H. L. Ploegh, T. R. Brummelkamp, Global
895 gene disruption in human cells to assign genes to phenotypes by deep sequencing. *Nat*
896 *Biotechnol* **29**, 542-546 (2011).
897 58. M. Jost, Y. Chen, L. A. Gilbert, M. A. Horlbeck, L. Krenning, G. Menchon, A. Rai, M. Y.
898 Cho, J. J. Stern, A. E. Prota, M. Kampmann, A. Akhmanova, M. O. Steinmetz, M. E.
899 Tanenbaum, J. S. Weissman, Combined CRISPRi/a-Based Chemical Genetic Screens
900 Reveal that Rigosertib Is a Microtubule-Destabilizing Agent. *Mol Cell* **68**, 210-223 e216
901 (2017).
902 59. http://weissmanlab.ucsf.edu/CRISPR/CRISPR.html. (2017).
903 60. T. R. Peterson, S. S. Sengupta, T. E. Harris, A. E. Carmack, S. A. Kang, E. Balderas, D.
904 A. Guertin, K. L. Madden, A. E. Carpenter, B. N. Finck, D. M. Sabatini, mTOR complex 1
905 regulates lipin 1 localization to control the SREBP pathway. *Cell* **146**, 408-420 (2011).
906 61. T. R. Peterson, M. Laplante, C. C. Thoreen, Y. Sancak, S. A. Kang, W. M. Kuehl, N. S.
907 Gray, D. M. Sabatini, DEPTOR is an mTOR inhibitor frequently overexpressed in
908 multiple myeloma cells and required for their survival. *Cell* **137**, 873-886 (2009).
909 62. F. A. Ran, P. D. Hsu, J. Wright, V. Agarwala, D. A. Scott, F. Zhang, Genome
910 engineering using the CRISPR-Cas9 system. *Nat Protoc* **8**, 2281-2308 (2013).
911 63. F. P. Coxon, M. H. Helfrich, R. Van't Hof, S. Sebti, S. H. Ralston, A. Hamilton, M. J.
912 Rogers, Protein geranylgeranylation is required for osteoclast formation, function, and
913 survival: inhibition by bisphosphonates and GGTI-298. *J Bone Miner Res* **15**, 1467-1476
914 (2000).
915 64. J. C. Frith, J. Monkkonen, S. Auriola, H. Monkkonen, M. J. Rogers, The molecular
916 mechanism of action of the antiresorptive and antiinflammatory drug clodronate:
917 evidence for the formation in vivo of a metabolite that inhibits bone resorption and

causes osteoclast and macrophage apoptosis. *Arthritis and rheumatism* **44**, 2201-2210 (2001).
65. M. Tsubaki, M. Komai, T. Itoh, M. Imano, K. Sakamoto, H. Shimaoka, T. Takeda, N. Ogawa, K. Mashimo, D. Fujiwara, J. Mukai, K. Sakaguchi, T. Satou, S. Nishida, Nitrogen-containing bisphosphonates inhibit RANKL- and M-CSF-induced osteoclast formation through the inhibition of ERK1/2 and Akt activation. *J Biomed Sci* **21**, 10 (2014).
66. R. Kuhn, R. M. Torres, Cre/loxP recombination system and gene targeting. *Methods Mol Biol* **180**, 175-204 (2002).
67. https://simple.wikipedia.org/wiki/Central_dogma_of_molecular_biology.
68. F. Schwenk, U. Baron, K. Rajewsky, A cre-transgenic mouse strain for the ubiquitous deletion of loxP-flanked gene segments including deletion in germ cells. *Nucleic Acids Res* **23**, 5080-5081 (1995).
69. C. F. Lai, S. L. Cheng, G. Mbalaviele, C. Donsante, M. Watkins, G. L. Radice, R. Civitelli, Accentuated ovariectomy-induced bone loss and altered osteogenesis in heterozygous N-cadherin null mice. *J Bone Miner Res* **21**, 1897-1906 (2006).
70. R. K. Fuchs, R. J. Phipps, D. B. Burr, Recovery of trabecular and cortical bone turnover after discontinuation of risedronate and alendronate therapy in ovariectomized rats. *J Bone Miner Res* **23**, 1689-1697 (2008).
71. M. R. Allen, K. Iwata, R. Phipps, D. B. Burr, Alterations in canine vertebral bone turnover, microdamage accumulation, and biomechanical properties following 1-year treatment with clinical treatment doses of risedronate or alendronate. *Bone* **39**, 872-879 (2006).
72. M. L. Bouxsein, K. S. Myers, K. L. Shultz, L. R. Donahue, C. J. Rosen, W. G. Beamer, Ovariectomy-induced bone loss varies among inbred strains of mice. *J Bone Miner Res* **20**, 1085-1092 (2005).
73. M. D. Willinghamm, M. D. Brodt, K. L. Lee, A. L. Stephens, J. Ye, M. J. Silva, Age-related changes in bone structure and strength in female and male BALB/c mice. *Calcif Tissue Int* **86**, 470-483 (2010).
74. S. K. Grimston, D. B. Goldberg, M. Watkins, M. D. Brodt, M. J. Silva, R. Civitelli, Connexin43 deficiency reduces the sensitivity of cortical bone to the effects of muscle paralysis. *J Bone Miner Res* **26**, 2151-2160 (2011).
75. T. A. Guise, Antitumor effects of bisphosphonates: promising preclinical evidence. *Cancer Treat Rev* **34 Suppl 1**, S19-24 (2008).
76. R. Aft, M. Naughton, K. Trinkaus, M. Watson, L. Ylagan, M. Chavez-MacGregor, J. Zhai, S. Kuo, W. Shannon, K. Diemer, V. Herrmann, J. Dietz, A. Ali, M. Ellis, P. Weiss, T. Eberlein, C. Ma, P. M. Fracasso, I. Zoberi, M. Taylor, W. Gillanders, T. Pluard, J. Mortimer, K. Weilbaecher, Effect of zoledronic acid on disseminated tumour cells in women with locally advanced breast cancer: an open label, randomised, phase 2 trial. *Lancet Oncol* **11**, 421-428 (2010).
77. B. M. Bolstad, R. A. Irizarry, M. Astrand, T. P. Speed, A comparison of normalization methods for high density oligonucleotide array data based on variance and bias. *Bioinformatics* **19**, 185-193 (2003).
78. C. V. Gentleman R, Huber W and Hahne F (2017).
79. G. K. Smyth, Linear models and empirical bayes methods for assessing differential expression in microarray experiments. *Stat Appl Genet Mol Biol* **3**, Article3 (2004).
80. M. Carlson. (2016).
81. J. G. Buchan, D. M. Alvarado, G. E. Haller, C. Cruchaga, M. B. Harms, T. Zhang, M. C. Willing, D. K. Grange, A. C. Braverman, N. H. Miller, J. A. Morcuende, N. L. Tang, T. P. Lam, B. K. Ng, J. C. Cheng, M. B. Dobbs, C. A. Gurnett, Rare variants in FBN1 and

FBN2 are associated with severe adolescent idiopathic scoliosis. *Hum Mol Genet* **23**, 5271-5282 (2014).

82. C. Cruchaga, C. M. Karch, S. C. Jin, B. A. Benitez, Y. Cai, R. Guerreiro, O. Harari, J. Norton, J. Budde, S. Bertelsen, A. T. Jeng, B. Cooper, T. Skorupa, D. Carrell, D. Levitch, S. Hsu, J. Choi, M. Ryten, J. Hardy, D. Trabzuni, M. E. Weale, A. Ramasamy, C. Smith, C. Sassi, J. Bras, J. R. Gibbs, D. G. Hernandez, M. K. Lupton, J. Powell, P. Forabosco, P. G. Ridge, C. D. Corcoran, J. T. Tschanz, M. C. Norton, R. G. Munger, C. Schmutz, M. Leary, F. Y. Demirci, M. N. Bamne, X. Wang, O. L. Lopez, M. Ganguli, C. Medway, J. Turton, J. Lord, A. Braae, I. Barber, K. Brown, P. Passmore, D. Craig, J. Johnston, B. McGuinness, S. Todd, R. Heun, H. Kolsch, P. G. Kehoe, N. M. Hooper, E. R. Vardy, D. M. Mann, S. Pickering-Brown, N. Kalsheker, J. Lowe, K. Morgan, A. David Smith, G. Wilcock, D. Warden, C. Holmes, P. Pastor, O. Lorenzo-Betancor, Z. Brkanac, E. Scott, E. Topol, E. Rogaeva, A. B. Singleton, M. I. Kamboh, P. St George-Hyslop, N. Cairns, J. C. Morris, J. S. Kauwe, A. M. Goate, Rare coding variants in the phospholipase D3 gene confer risk for Alzheimer's disease. *Nature* **505**, 550-554 (2014).

83. P. Krawitz, C. Rodelsperger, M. Jager, L. Jostins, S. Bauer, P. N. Robinson, Microindel detection in short-read sequence data. *Bioinformatics* **26**, 722-729 (2010).

84. A. McKenna, M. Hanna, E. Banks, A. Sivachenko, K. Cibulskis, A. Kernytsky, K. Garimella, D. Altshuler, S. Gabriel, M. Daly, M. A. DePristo, The Genome Analysis Toolkit: a MapReduce framework for analyzing next-generation DNA sequencing data. *Genome Res* **20**, 1297-1303 (2010).

85. G. A. Van der Auwera, M. O. Carneiro, C. Hartl, R. Poplin, G. Del Angel, A. Levy-Moonshine, T. Jordan, K. Shakir, D. Roazen, J. Thibault, E. Banks, K. V. Garimella, D. Altshuler, S. Gabriel, M. A. DePristo, From FastQ data to high confidence variant calls: the Genome Analysis Toolkit best practices pipeline. *Curr Protoc Bioinformatics* **43**, 11 10 11-33 (2013).

86. M. Lek, K. J. Karczewski, E. V. Minikel, K. E. Samocha, E. Banks, T. Fennell, A. H. O'Donnell-Luria, J. S. Ware, A. J. Hill, B. B. Cummings, T. Tukiainen, D. P. Birnbaum, J. A. Kosmicki, L. E. Duncan, K. Estrada, F. Zhao, J. Zou, E. Pierce-Hoffman, J. Berghout, D. N. Cooper, N. Deflaux, M. DePristo, R. Do, J. Flannick, M. Fromer, L. Gauthier, J. Goldstein, N. Gupta, D. Howrigan, A. Kiezun, M. I. Kurki, A. L. Moonshine, P. Natarajan, L. Orozco, G. M. Peloso, R. Poplin, M. A. Rivas, V. Ruano-Rubio, S. A. Rose, D. M. Ruderfer, K. Shakir, P. D. Stenson, C. Stevens, B. P. Thomas, G. Tiao, M. T. Tusie-Luna, B. Weisburd, H. H. Won, D. Yu, D. M. Altshuler, D. Ardissino, M. Boehnke, J. Danesh, S. Donnelly, R. Elosua, J. C. Florez, S. B. Gabriel, G. Getz, S. J. Glatt, C. M. Hultman, S. Kathiresan, M. Laakso, S. McCarroll, M. I. McCarthy, D. McGovern, R. McPherson, B. M. Neale, A. Palotie, S. M. Purcell, D. Saleheen, J. M. Scharf, P. Sklar, P. F. Sullivan, J. Tuomilehto, M. T. Tsuang, H. C. Watkins, J. G. Wilson, M. J. Daly, D. G. MacArthur, C. Exome Aggregation, Analysis of protein-coding genetic variation in 60,706 humans. *Nature* **536**, 285-291 (2016).

Acknowledgements: We thank members of the Peterson and Erin O'Shea laboratories for helpful discussions, especially Chris Chow and Kevin Li (Peterson); and A. R. Subramaniam, Christopher Chidley, and Anna Puszynska for illustrations (O'Shea). We thank Mary Bouxsein and Daniel Brooks (Beth Israel Deaconess Medical Center), and Dan Lieb, Yung Kim, and Matt

1014 Silva (Washington University School of Medicine) for bone structure and function analysis. We
1015 thank Kenichi Nagano and Roland Baron (Harvard School of Dental Medicine), Yoshiko
1016 Iwamoto (Massachusetts General Hospital) and Deb Novack, Gary London, Krzysztof Hyrc, and
1017 Crystal Idleburg for histology, histomorphometry, and imaging (Washington University School of
1018 Medicine). Luke Gilbert (University of California San Francisco) for assistance on the CRISPRi/a
1019 screening protocol. **Funding:** This work was supported by grants from the NIH (CA103866 and
1020 AI047389 to D.M.S., HD070394 to B.L.) and Department of Defense (W81XWH-07-0448 to
1021 D.M.S.); awards from the W.M. Keck Foundation and the LAM (lymphangioleiomyomatosis)
1022 Foundation to D.M.S.; Rolanette and Berdon Lawrence Bone Disease Program of Texas and
1023 BCM Center for Skeletal Medicine and Biology and NIDDK training grant 5T32DK060445-10 to
1024 A.R.; fellowships from the Jane Coffin Childs Foundation, NIH/NIA K99/R00 AG047255,
1025 NIH/NIAMS R01 AR073017, and NIH/NIAMS P30 AR057235 to T.R.P; NIH/NIAMS K99
1026 AR073903 to L.E.S. D.M.S. is an investigator of the Howard Hughes Medical Institute. NCI
1027 2RO1CA129933 to D.A.H., who is also investigator of the Howard Hughes Medical Institute and
1028 a F30 NIH training grant to C.L.C. **Author Contributions:** T.R.P. and L.E.S. designed the
1029 study. D.T.B. performed the co-culture experiments and senile osteoporosis mouse studies.
1030 L.E.S. and J.L. performed the *ATRAID* variant studies. J.P., A.R., and Z.Y. performed viability
1031 assays. S.K. and L.E.S. performed immunoblots. Y.B., B.H.L, D.T.B. and N.S. conducted
1032 analysis of both basal and OVX mouse studies. C.L., F.W., and T.R.P. performed statistical
1033 analysis for the patient gene expression and mouse studies. T.R.P. performed the statistical
1034 analysis for the CRISPRi/a screens. S.M., J.C.B., M.M., M.S., M.H., S.D., V.N.B., R.C., M.J.G.,
1035 C.M.M., W.M.R., C.A.G., and K.D. performed the exome sequencing on the AFF patients. G.H.
1036 and C.C.G. performed statistical analysis for the exome sequencing of the AFF patients. D.A.H,
1037 C.L.C., K.M.S., N.R., T.B.D., and T.R.P. performed the exome sequencing on the ONJ patients.
1038 G.H. performed the statistical analysis for the exome sequencing of the ONJ patients. M.V.,
1039 K.B., J.E.C., T.R.B., D.M.S., and J.L. performed and/or provided assistance with the cell-based

genomic screening. T.R.P., J.P., and L.E.S. wrote the paper. **Competing Interests:** ATRAID, SNTG1, EPHB1, and PLCL1, the genes identified here, are part of a Whitehead–Harvard patent on which T.R.P., T.R.B., and D.M.S. are inventors. Shared reagents are subject to a materials transfer agreement. **Data and materials availability:** All data that supports the findings is available in the Figures, supplemental figures and tables.

Figures:

Fig. 1. *ATRAID* is required for molecular responses to nitrogen-containing bisphosphonates. (A) Schematic of haploid mutagenesis screening pipeline. Sequencing-based identification of gene-trap insertion sites in alendronate-resistant human haploid KBM7 cells. Genomic DNA for sequencing was obtained from mutagenized KBM7 cells grown for four weeks post-treatment with 165 μM alendronate. **(B)** Sequencing-based identification of gene-trap insertion sites in alendronate-resistant cells. N=number of unique insertions within the stated gene locus. False discovery rate corrected (FDR) p-values for *ATRAID*=7.02×10^{-45}, *PLCL1*=1.02×10^{-04}, *EPHB1*=2.05×10^{-04}, *SNTG1*= 1.84×10^{-03}. P-values represent enrichment in alendronate-treated versus vehicle treated cells. The red dotted line indicates the genes with a FDR p-value of < 0.05. 185 genes in this screen that met that criteria. **(C)** Schematic representation of structural features of human ATRAID protein and its mouse and frog orthologues. **(D)** Cell viability in wild-type control and *ATRAID*-deficient cells exogenously expressing or not expressing *ATRAID* cDNA. Cells were treated with 60 μM alendronate and analyzed for cell viability. Cell viability was determined by measuring cellular ATP levels and is expressed as a ratio of that compared with untreated cells. Error bars indicate the standard deviation for n=4 (biological replicates). N.S., not significant; * indicates p<0.05. v2, variant 2 (NM_080592.3); v3, variant 3 (NM_001170795.1) of the *ATRAID* gene, respectively. **(E)** Chemical structures for nitrogen-containing bisphosphonates (N-BPs) or non-nitrogen-containing bisphosphonates (BP) used in (E) are shown. KBM7 cell viability in *ATRAID*-deficient

1066 (ATRAID_GT1 and ATRAID_GT2) and control (wild-type) KBM7 cells upon treatment with
1067 nitrogen-containing bisphosphonates (N-BPs) or non-nitrogen-containing bisphosphonates (BP).
1068 All cells were treated with the indicated concentration of the indicated N-BP (alendronate,
1069 zoledronate), BP (etidronate, tiludronate) for 72 hours. Cell viability was determined by
1070 measuring cellular ATP levels and is expressed as a ratio of that compared with untreated cells.
1071 All measurements were performed in quadruplicate (biological replicates). * indicates $p<0.05$,
1072 unpaired *t*-test. **(F)** Alendronate induced inhibition of protein prenylation requires *ATRAID*.
1073 *ATRAID* deficient and *ATRAID* v3-reconstituted HEK-293T cells were treated with the indicated
1074 dose of alendronate for 24 hours then lysed and analyzed by immunoblotting for the indicated
1075 proteins. Equal amounts of protein were loaded in each lane. This experiment was repeated
1076 three times (biological replicates) and was consistent all three times. * indicates non-specific
1077 band.
1078
1079 **Fig. 2. ATRAID is required for organismal responses to nitrogen-containing**
1080 **bisphosphonates. (A)** Schematic of menopausal bone loss model – bilateral ovariectomy
1081 (OVX). Saline or 100 µg/kg/week alendronate was administered concurrent with OVX or a sham
1082 procedure. After four weeks, mice were euthanized and bones and serum were extracted and
1083 analyzed. **(B)** Representative µCT reconstructions of femoral trabecular bone from 4-month-old
1084 litter-matched derived, wild-type, *ATRAID* WT (+/+), and KO (-/-), female mice that were either
1085 ovariectomized (OVX) or sham operated (Sham), treated with either vehicle (saline) (+OVX), or
1086 alendronate (+OVX+ALN) for four weeks. **(C-F)** Ovariectomized *ATRAID*$^{-/-}$ mice have impaired
1087 bone microstructural responses to alendronate. Femur cortical (C, D) and trabeculae (E, F)
1088 regions were analyzed by µCT. Each circle represents an individual animal. Circles offset to the
1089 right represent unique animals with similar values to those of another animal (offset for visual
1090 clarity). N=6-11 mice (3.5 month old) per group. * indicates $p<0.01$, # indicates $0.01<p<0.05$, and
1091 red line indicates mean. **(G-H)** Ovariectomized *ATRAID* KO mice have impaired bone strength

1092 responses to alendronate. Stiffness (G) and yield load (H) were analyzed by three-point bending
1093 test. Each circle represents an individual animal. Circles offset to the right represent unique
1094 animals with similar values to those of another animal (offset for visual clarity). N=6-11 mice per
1095 group. *indicates $p<0.01$, #indicates $0.01<p<0.05$, N.S., indicates not significant, and red line
1096 indicates mean.
1097
1098 **Fig. 3. *ATRAID* is required cell-autonomously for N-BP inhibition of osteoclast**
1099 **prenylation.**
1100 **(A)** CTX-I, a serum marker of osteoclast activity is reduced in WT but not ATRAID KO
1101 ovariectomized mice by alendronate treatment. Serum CTX-I was measured by ELISA. Each
1102 circle represents an individual animal. Circles offset to the right represent unique animals with
1103 similar values to those of another animal (offset for visual clarity). N=8-13 mice per group. *
1104 indicates $p<0.05$. **(B)** Osteoclast histomorphometric responses are reduced in WT but not
1105 ATRAID KO ovariectomized mice by alendronate treatment. Osteoclast surface to bone surface
1106 ratio (Oc.S/BS) was determined by Tartrate Acid Phosphatase (TRAP)-assay reactivity. Each
1107 circle represents an individual animal. Circles offset to the right represent unique animals with
1108 similar values to those of another animal (offset for visual clarity). N=5-7 mice per group. *
1109 indicates $p<0.05$, n.s. indicates not significant, and red line indicates mean. **(C)** Quantitative
1110 PCR to examine mRNA expression of markers of osteoclast differentiation, *CTSK, RANK,*
1111 *TRAP,* in wild-type (WT) and ATRAID^{KO} cells M-CSF expanded, bone marrow macrophages
1112 (BMMs) differentiated with *RANKL* to osteoclasts. Expression is normalized to wild-type,
1113 undifferentiated BMM cells, using *ACTB* and *RPLP0* as control genes. Error bars represent the
1114 standard deviation of technical triplicate reactions. **(D)** Percent of Annexin-V positive cells after
1115 a 48 hour alendronate treatment of *ATRAID* WT (+/+) and KO (-/-) BMMs differentiated into
1116 osteoclasts. Annexin V staining was assessed using flow cytometry. Each circle represents
1117 osteoclasts derived from an individual animal (split for treatment with 0, 10μM, 30μM

1118 alendronate). Red line indicates mean. * indicates p<0.05, N.S. indicates not significant. **(E)**
1119 Percent of Annexin-V positive cells after a 48 hour alendronate treatment (0, 30μM, 80μM) in
1120 wild-type and *ATRAID*^{KO} differentiated RAW 264.7 osteoclasts. Annexin V staining was
1121 assessed using flow cytometry. Error bars represent the standard deviation of n=3 experiments
1122 (biological replicates), * indicates p<0.05. **(F)** Immunoblots of cell lysates of RAW wild-type (WT)
1123 and *ATRAID*^{KO} (KO) cells, and RAW 264.7-derived osteoclasts treated with alendronate for 48
1124 hours, demonstrating *ATRAID* deficiency confers resistance to alendronate-induced prenylation
1125 defects. Top panel: immunoblot specific to the unprenylated version of Rap1a. Bottom panel:
1126 Gapdh, serving as a loading control. Alendronate concentrations were 0, 20μM, 80μM. **(G)**
1127 Representative image of a six-well dish co-culture of equal numbers of mouse primary
1128 osteoblasts and osteoclasts of the indicated genotypes with or without the indicated doses of
1129 alendronate (ALN) for four days. The experiment was performed three independent times with a
1130 similar result. Red staining reflects TRAP-assay reactivity. **(H)** Image analysis of the samples in
1131 (G). Error bars represent the standard deviation of n=3 independent images (technical
1132 replicates). * indicates p<0.01, N.S. indicates not significant.
1133
1134 **Fig. 4. *ATRAID* as a potential genetic factor for altered responses to nitrogen-containing**
1135 **bisphosphonates in patients. (A)** Genome-wide studies of N-BP responsiveness in patients
1136 vs. cells. The outcomes considered from human studies involving N-BPs are: osteonecrosis of
1137 the jaw (ONJ), breast cancer bone marrow micrometastases (i.e., disseminated tumor cells
1138 (DTC)), and atypical femoral fractures (AFF). *ATRAID, ATR, ZBTB4* are statistically significant
1139 hits (p < 0.05) in N-BP cell-based CRISPRi/a screening, differentially expressed in both gene
1140 expression datasets (ONJ and DTC), and possess rare multiple non-synonymous coding
1141 variants in AFF and ONJ cases but not controls. These three genes are visualized as the Venn
1142 diagram of overlap of lists of genes that met the following criteria: significant alendronate
1143 CRISPRi, zoledronate CRISPRi, or alendronate CRISPRa hits with absolute value of rho growth

1144 phenotype values >= 0.30 and p <= 0.05 (1335 out of 15828 genes) (*19, 45*); differentially
1145 expressed N-BP in ONJ + DTC (774 out of 18415 for ONJ (*43*) and 20492 for DTC (*44*);
1146 multiple coding variant(s) in AFF and ONJ cases and not controls (1252 out of 11659 genes)
1147 (data as part of this study). **(B)** Patient genetic data for *ATRAID*. Raw expression values were
1148 normalized to 1 to fit on a comparable Y axis. * indicates p<0.05. N.S. indicates not significant.
1149 "X"-enriched refers to the fold-enrichment of the allele compared with a population with a similar
1150 genetic background as the cases. For example, for *ATRAID*, the D5G variant is present in 2 out
1151 of 27 AFF patients. Though this allele wasn't detected in the 11 control samples, it is present in
1152 a population of European Americans (EA) and Asian Americans (AA) that is representative of
1153 the study population at a prevalence of 0.0131. Therefore, the D5G allele is (2/27) / 0.0131 =
1154 5.66X enriched in cases compared to the EA/AA population. "v3" and "v2" refer to isoforms of
1155 the *ATRAID* gene. A simple binomial test was used to calculate the significance of each variant.
1156 * indicates p<0.05. **(C)** Quantitative PCR to examine *ATRAID* mRNA expression in wild-type,
1157 ATRAID deficient, and low ATRAID expressing cells. Error bars represent the standard
1158 deviation of technical triplicate reactions. Expression was normalized to WT cells using *RPLP0*
1159 and *TBP* as controls. **(D)** Cell viability in wild-type, *ATRAID* deficient, and low *ATRAID*
1160 expressing cells. Cells were treated with the indicated doses of alendronate and analyzed for
1161 cell viability. Cell viability was determined by measuring cellular ATP levels and is expressed as
1162 a ratio of that compared with untreated cells. Error bars indicate the standard deviation for n=4
1163 (biological replicates). N.S., not significant; * and # indicate p<0.05 for the indicated cell lines.
1164 **(E)** Immunoblot of wild-type and D5G/G32R variant *ATRAID*-V5 tagged proteins. Mutant or wild-
1165 type *ATRAID* v2 and v3 were stably introduced into *ATRAID* deficient HEK-293T cells. **(F)** Cell
1166 viability in wild-type vs. D5G/G32R variant cells. Cells were treated with the indicated doses of
1167 alendronate and analyzed for cell viability. Cell viability was determined by measuring cellular
1168 ATP levels and is expressed as a ratio of that compared with untreated cells. Error bars indicate
1169 the standard deviation for n=4 (biological replicates). N.S., not significant; * indicates p<0.05.

1170

1171 **Supplementary Materials:**

1172 **Fig. S1, related to Fig. 1. ATRAID is required for cellular responses to nitrogen-containing**
1173 **bisphosphonates. (A)** Schematic of the exon structure of the three human *ATRAID* mRNA
1174 variants. The coding sequence for each variant is in green. Non-coding portions of each exon
1175 are in grey. The translated regions of variant 1 and variant 3 are shorter than variant 2 due to
1176 internal translation initiation sites. The location of the primer sets used to identify each *ATRAID*
1177 gene trap (GT) are indicated (in blue for ATRAID_GT1; in red for ATRAID_GT2). **(B)** mRNA
1178 analysis of *ATRAID* and *GGPS1* expression levels in clones that contain independent gene-trap
1179 insertions in their respective loci. Wild-type KBM7 cells were compared with mutant alleles
1180 (labeled as GT) and *GGPS1* was used as a loading control. **(C)** *ATRAID* deficient cells are
1181 resistant to alendronate over a wide range of concentrations and cell numbers. KBM7 cell
1182 viability was determined by measuring cellular ATP levels and is expressed as a ratio of that
1183 compared with untreated cells. All measurements were performed in quadruplicate (biological
1184 replicates). * indicates $p<0.05$, unpaired t-test. **(D)** Untreated WT and *ATRAID* deficient cells
1185 grow at a similar rate. WT and *ATRAID* deficient HEK-293T cells were plated at the same cell
1186 density (10,000 cells/per well), allowed to grow for 48 hours, and ATP levels were measured.
1187 Viability measurements were performed in quadruplicate (biological replicates). Error bars
1188 reflect standard deviation. **(E)** *ATRAID* overexpression sensitizes cells to alendronate. HEK-
1189 293T cells were transfected with either Metap2 (control), or ATRAID-cDNA expressing vectors
1190 and the indicated doses of alendronate for 72 hours. Viability measurements were performed in
1191 quadruplicate (biological replicates). * indicates $p<0.05$, unpaired t-test. **(F)** Alendronate
1192 regulation of viability is dependent on ATRAID membrane targeting. Cells deficient in ATRAID
1193 (ATRAID_GT2) were transformed to express exogenous Metap2 (control), tubulin (control),
1194 ATRAID variant 2 (_v2), or ATRAID variant 2 lacking the transmembrane domain (Δmem_v2).
1195 Cells were treated with alendronate at the indicated dose for 72 hours. Cell viability was

1196 determined as in $p<0.05$, unpaired t-test (n=6) (3 biological replicates, 3 technical replicates).
1197 **(G)** An additional cell line whose alendronate-dependent regulation of prenylation requires
1198 *ATRAID*. Wild-type control and *ATRAID* deficient KBM7 cells exogenously expressing or not
1199 expressing *ATRAID* cDNA were treated with the indicated dose of alendronate for 24 hours then
1200 lysed and analyzed by immunoblotting for the indicated proteins. Equal amounts of protein were
1201 loaded in each lane. This experiment was repeated three times (biological replicates) and was
1202 consistent all three times.
1203
1204 **Fig. S2, related to Fig. 2. ATRAID is required for organismal responses to nitrogen-**
1205 **containing bisphosphonates.**
1206 **(A)** Schematic of *ATRAID* targeted gene locus and genotyping strategy. *ATRAID* exon 3-exon 5
1207 are targeted, i.e., flanked by LoxP sites. **(B)** Confirmation of deletion of protein-coding genomic
1208 DNA at the *ATRAID* gene locus. WT, wild-type at the *ATRAID* locus; het, heterozygous; KO,
1209 homozygous deletion. **(C)** *ATRAID* KO mice have reduced body weight compared with *ATRAID*
1210 wild-type WT (+/+) mice. N=6-13 for wild-type, N=7-14 for ATRAID KO mice. * indicates $p<0.05$.
1211 **(D)** Cells from *ATRAID* KO mice lack *ATRAID* mRNA. Tail fibroblast cells were analyzed for
1212 mRNA expression of *ATRAID* by RT-PCR and normalized to RPLP0 mRNA levels. Error bars
1213 indicate standard deviation for n=4 (biological replicates). * indicates $p<0.05$, unpaired t-test. **(E)**
1214 Cells from the tails of *ATRAID* KO animals are resistant to the cytotoxic effects of alendronate.
1215 All cells were treated with the indicated concentration of alendronate for 72 hours. Cell viability
1216 was determined by measuring cellular ATP levels and is expressed as a ratio of that compared
1217 with untreated cells. All measurements were performed in quadruplicate (biological replicates). *
1218 indicates $p<0.05$, unpaired t-test. **(F)** *ATRAID* mRNA is undetectable in tibia of ATRAID
1219 knockout mice. Tibias were analyzed for *ATRAID* mRNA expression by RT-qPCR and
1220 normalized to RPLP0 mRNA levels. Error bars indicate standard deviation for n=4 (biological
1221 replicates). * indicates $p<0.05$, unpaired t-test. **(G)** Femurs from *ATRAID* KO mice are slightly

1222 smaller but grossly morphologically normal. Representative traverse μCT images at the femoral
1223 distal metaphysis from wild-type and *ATRAID* KO mice. Femur lengths in millimeters (mm) were
1224 based on μCT measurement. Error measurements are standard deviation for n=5-6 mice. *
1225 indicates p<0.05, unpaired t-test. **(H, I)** *ATRAID* KO mice bone microstructure isn't significantly
1226 altered. Femur trabeculae (H) and cortical (I) regions were analyzed by μCT. Each circle
1227 represents an individual animal. Circles offset to the right represent unique animals with similar
1228 values to those of another animal (offset for visual clarity). N=8-10 (2-month-old) mice per
1229 group. n.s. indicates not significant, unpaired t-test. **(J-L)** ATRAID KO mice have impaired bone
1230 strength. Stiffness (J), yield load (K), and post-yield displacement (L) were analyzed by three-
1231 point bending test. Each circle represents an individual animal. Circles offset to the right
1232 represent unique animals with similar values to those of another animal (offset for visual clarity).
1233 N=8-10 mice (2-month-old) per group. * indicates p<0.05, n.s. indicates not significant, unpaired
1234 t-test. **(M, N)** Markers of osteoclast function aren't significant different comparing ATRAID wild-
1235 type, WT (+/+) with knockout, KO (-/-) mice. (M) Serum C-terminal telopeptides of type I
1236 collagen (CTX-I) were measured in serum obtained from 3-month-old males using ELISA. Each
1237 circle represents an individual animal. Circles offset to the right represent unique animals with
1238 similar values to those of another animal (offset for visual clarity). N=6 mice per group. n.s.
1239 indicates not significant, unpaired t-test. (N) Osteoclast surface to bone surface ratio (Oc.S/BS)
1240 was determined by Tartrate Acid Phosphatase (TRAP)-assay reactivity. Each circle represents
1241 an individual animal. Circles offset to the right represent unique animals with similar values to
1242 those of another animal (offset for visual clarity). N=6 mice per group. n.s. indicates not
1243 significant, unpaired t-test. **(O, P)** *ATRAID* KO mice have altered markers of osteoblast function.
1244 (O) Gla-Osteocalcin was measured in serum obtained from 3-month-old males using ELISA.
1245 Each circle represents an individual animal. Circles offset to the right represent unique animals
1246 with similar values to those of another animal (offset for visual clarity). N=7-9 mice per group. *
1247 indicates p<0.05, unpaired t-test. (P) bone formation rate (BFR/BS) determined by double

1248 labeling using calcein followed by alizarin red were analyzed histologically. Each circle
1249 represents an individual animal. Circles offset to the right represent unique animals with similar
1250 values to those of another animal (offset for visual clarity). N=5-7 mice per group. * indicates
1251 p<0.05, n.s. indicates not significant, unpaired t-test. **(Q, R)** Senile osteoporotic (18 month old)
1252 *ATRAID* deficient mice have impaired bone microstructural responses to alendronate. Femur
1253 trabeculae regions from WT and *ATRAID* KO mice were analyzed by μCT. Each circle
1254 represents an individual animal. Circles offset to the right represent unique animals with similar
1255 values to those of another animal (offset for visual clarity). N=5-8 mice per group. * indicates
1256 p<0.05, and red line indicates mean.
1257
1258 **Fig. S3, related to Fig. 3. *ATRAID* required cell-autonomously for N-BP inhibition of**
1259 **osteoclast prenylation.**
1260 **(A, B)** Osteoclast surface and numbers are reduced in WT but not *ATRAID* KO ovariectomized
1261 or senile mice by alendronate treatment. Osteoclast surface per bone surface (Oc.S/BS) (A) and
1262 the number of osteoclasts per bone surface (N.Oc/BS) (B) were determined by Tartrate-
1263 Resistant Acid Phosphatase (TRAP)-assay reactivity. Each circle represents an individual
1264 animal. Circles offset to the right represent unique animals with similar values to those of
1265 another animal (offset for visual clarity). N=5-7 mice per group (OVX); N=4-7 mice per group
1266 (senile). * indicates p<0.05, n.s. indicates not significant, and red line indicates mean. **(C, D)**
1267 Osteoblast function isn't significantly altered by alendronate in WT or *ATRAID* KO
1268 ovariectomized or senile mice. Mineral apposition rate (MAR) (C) and bone formation rate
1269 (BFR/BS) (D) were determined by double labeling using Calcein followed by Alizarin Red were
1270 analyzed histologically. Each circle represents an individual animal. Circles offset to the right
1271 represent unique animals with similar values to those of another animal (offset for visual clarity).
1272 N=5-7 mice per group (OVX); N=4-7 mice per group (senile). * indicates p<0.05, n.s. indicates
1273 not significant, and red line indicates mean. **(E)** Schematic of the mouse *ATRAID* first coding

1274 exon, indicating the CRISPR-induced mutations present in the two *ATRAID*^{KO} clones used in

1275 Fig. 3.

Figure 1

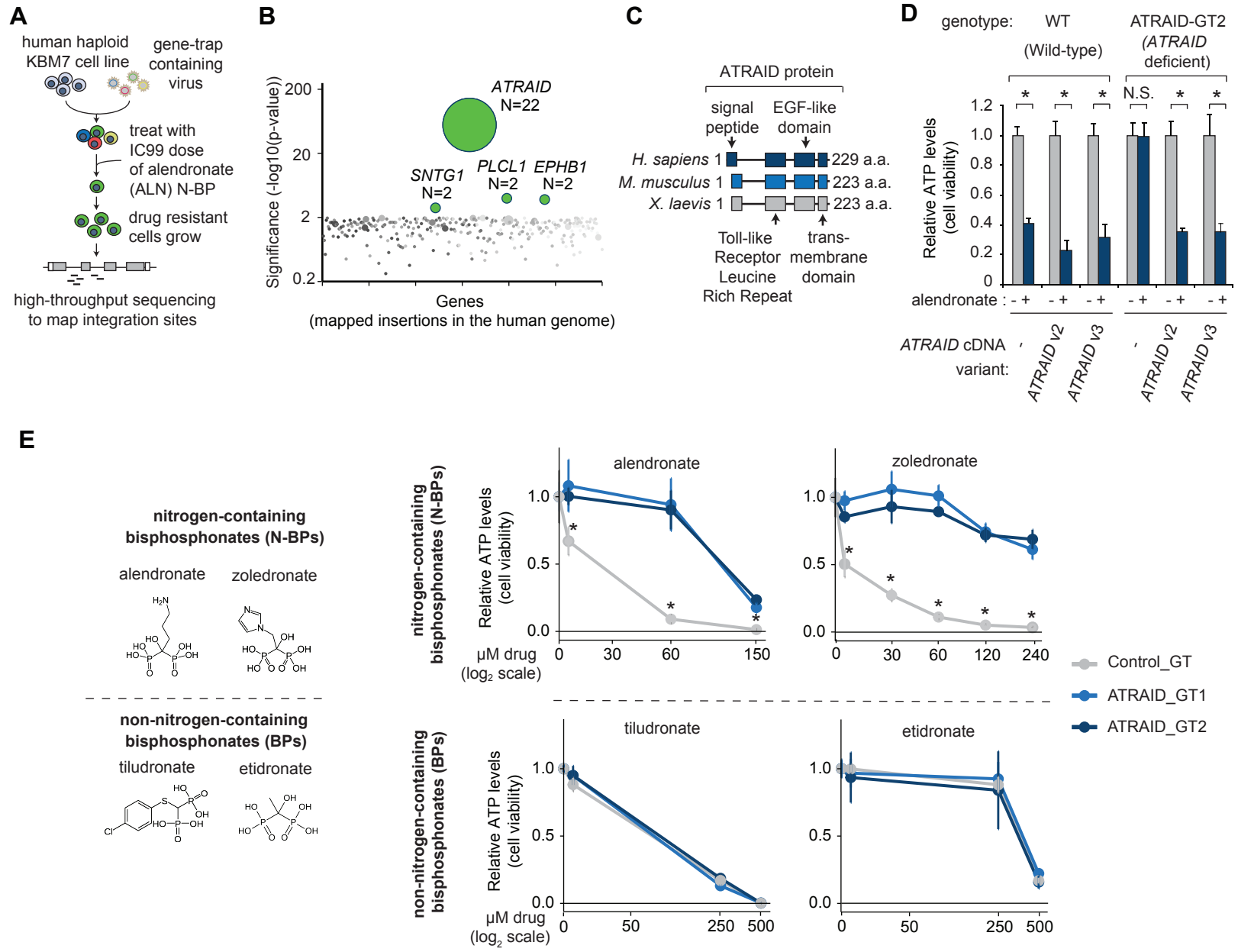
A
human haploid KBM7 cell line
gene-trap containing virus
treat with IC99 dose of alendronate (ALN) N-BP
drug resistant cells grow
high-throughput sequencing to map integration sites
B
Significance (-log10(p-value))
ATRAID N=22
SNTG1 N=2
PLCL1 N=2
EPHB1 N=2
Genes (mapped insertions in the human genome)
C
ATRAID protein
signal peptide
EGF-like domain
H. sapiens 1
M. musculus 1
X. laevis 1
229 a.a.
223 a.a.
223 a.a.
Toll-like Receptor Leucine Rich Repeat
trans-membrane domain
D
genotype:
WT (Wild-type)
ATRAID-GT2 (ATRAID deficient)
N.S.
Relative ATP levels (cell viability)
alendronate :
ATRAID cDNA variant:
ATRAID v2
ATRAID v3
E
nitrogen-containing bisphosphonates (N-BPs)
alendronate
zoledronate
non-nitrogen-containing bisphosphonates (BPs)
tiludronate
etidronate
nitrogen-containing bisphosphonates (N-BPs)
non-nitrogen-containing bisphosphonates (BPs)
Relative ATP levels (cell viability)
μM drug (log2 scale)
Control_GT
ATRAID_GT1
ATRAID_GT2
F
genotype:
ATRAID_KO (ATRAID deficient)
ATRAID cDNA variant:
v3
-
alendronate (μM):
(unprenylated) Rap1a
HDJ-2
unprenylated
prenylated
GAPDH
ATRAID-FLAG

Figure 2

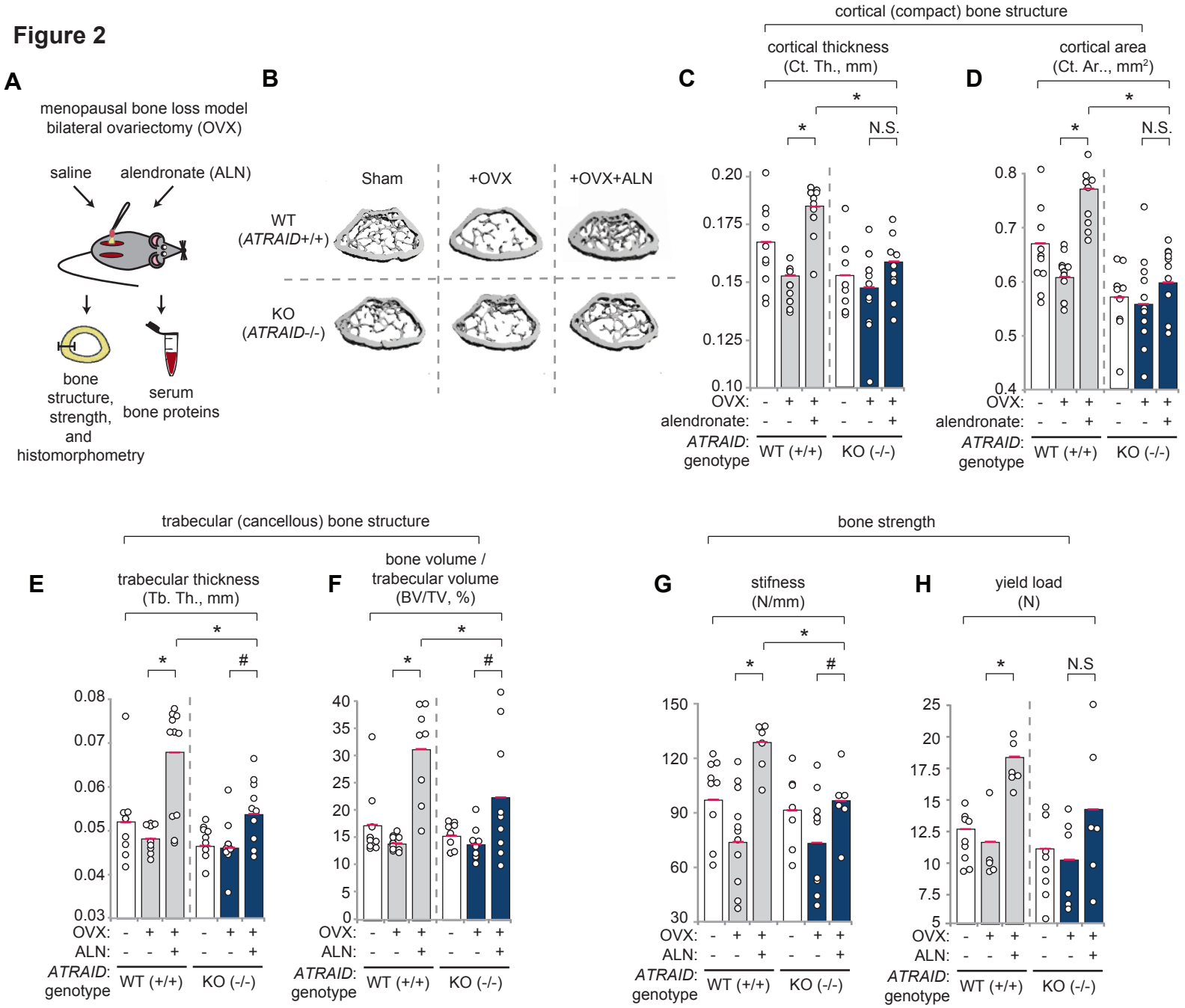
A
menopausal bone loss model
bilateral ovariectomy (OVX)
saline
alendronate (ALN)
bone structure, strength, and histomorphometry
serum bone proteins
B
Sham
+OVX
+OVX+ALN
WT (ATRAID+/+)
KO (ATRAID-/-)
C
cortical (compact) bone structure
cortical thickness (Ct. Th., mm)
D
cortical area (Ct. Ar.., mm²)
OVX:
alendronate:
ATRAID: genotype
WT (+/+)
KO (-/-)
N.S.
E
trabecular (cancellous) bone structure
trabecular thickness (Tb. Th., mm)
F
bone volume / trabecular volume (BV/TV, %)
ALN:
G
bone strength
stifness (N/mm)
H
yield load (N)

Figure 3

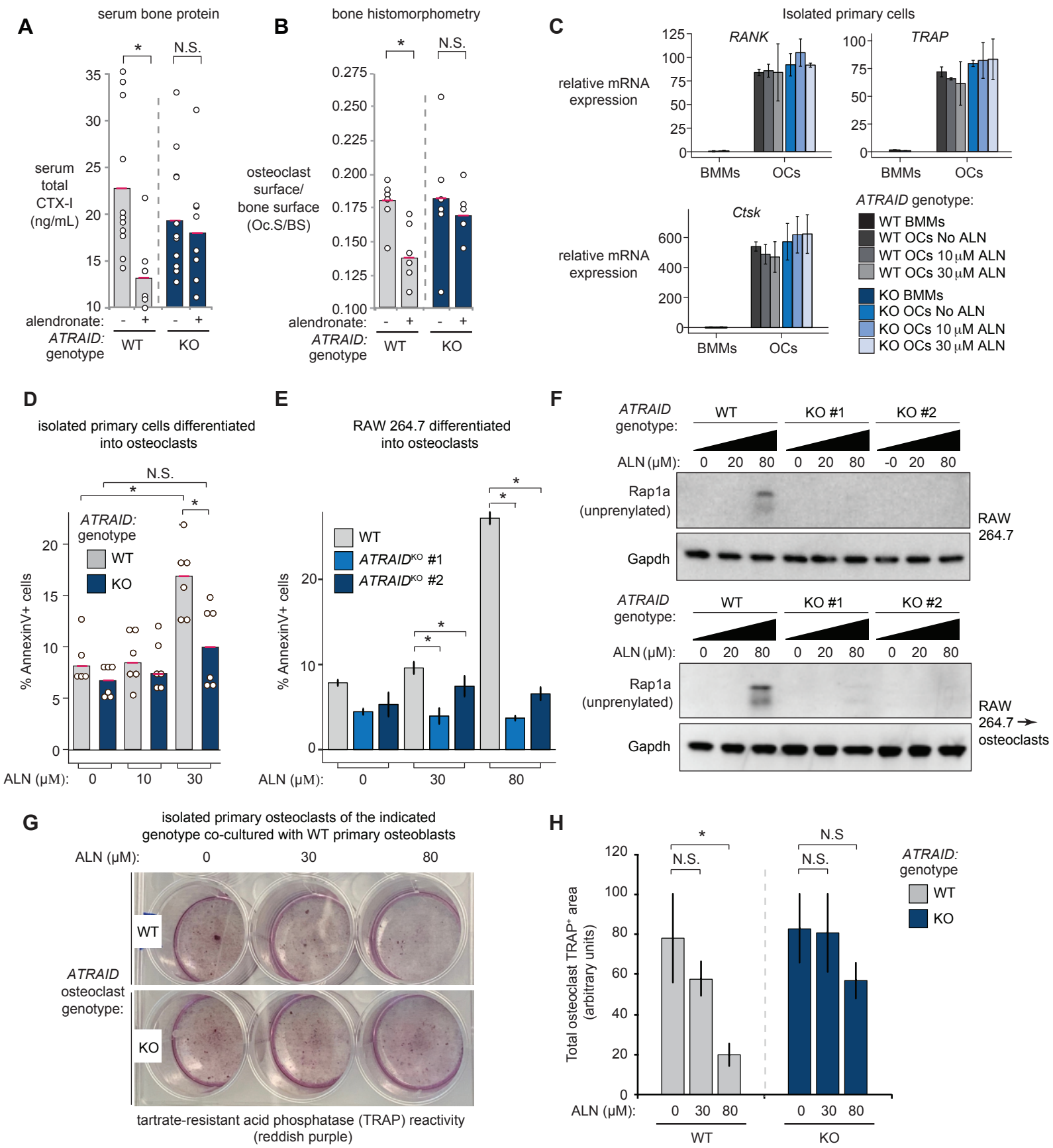
A
serum bone protein
serum total CTX-I (ng/mL)
alendronate:
ATRAID: genotype
WT
KO
B
bone histomorphometry
osteoclast surface/ bone surface (Oc.S/BS)
C
Isolated primary cells
RANK
TRAP
Ctsk
relative mRNA expression
BMMs
OCs
ATRAID genotype:
WT BMMs
WT OCs No ALN
WT OCs 10 μM ALN
WT OCs 30 μM ALN
KO BMMs
KO OCs No ALN
KO OCs 10 μM ALN
KO OCs 30 μM ALN
D
isolated primary cells differentiated into osteoclasts
% AnnexinV+ cells
ALN (μM):
E
RAW 264.7 differentiated into osteoclasts
ATRAIDKO #1
ATRAIDKO #2
F
ATRAID genotype:
KO #1
KO #2
Rap1a (unprenylated)
Gapdh
RAW 264.7
RAW 264.7 → osteoclasts
G
isolated primary osteoclasts of the indicated genotype co-cultured with WT primary osteoblasts
ATRAID osteoclast genotype:
tartrate-resistant acid phosphatase (TRAP) reactivity (reddish purple)
H
Total osteoclast TRAP+ area (arbitrary units)

Figure 4

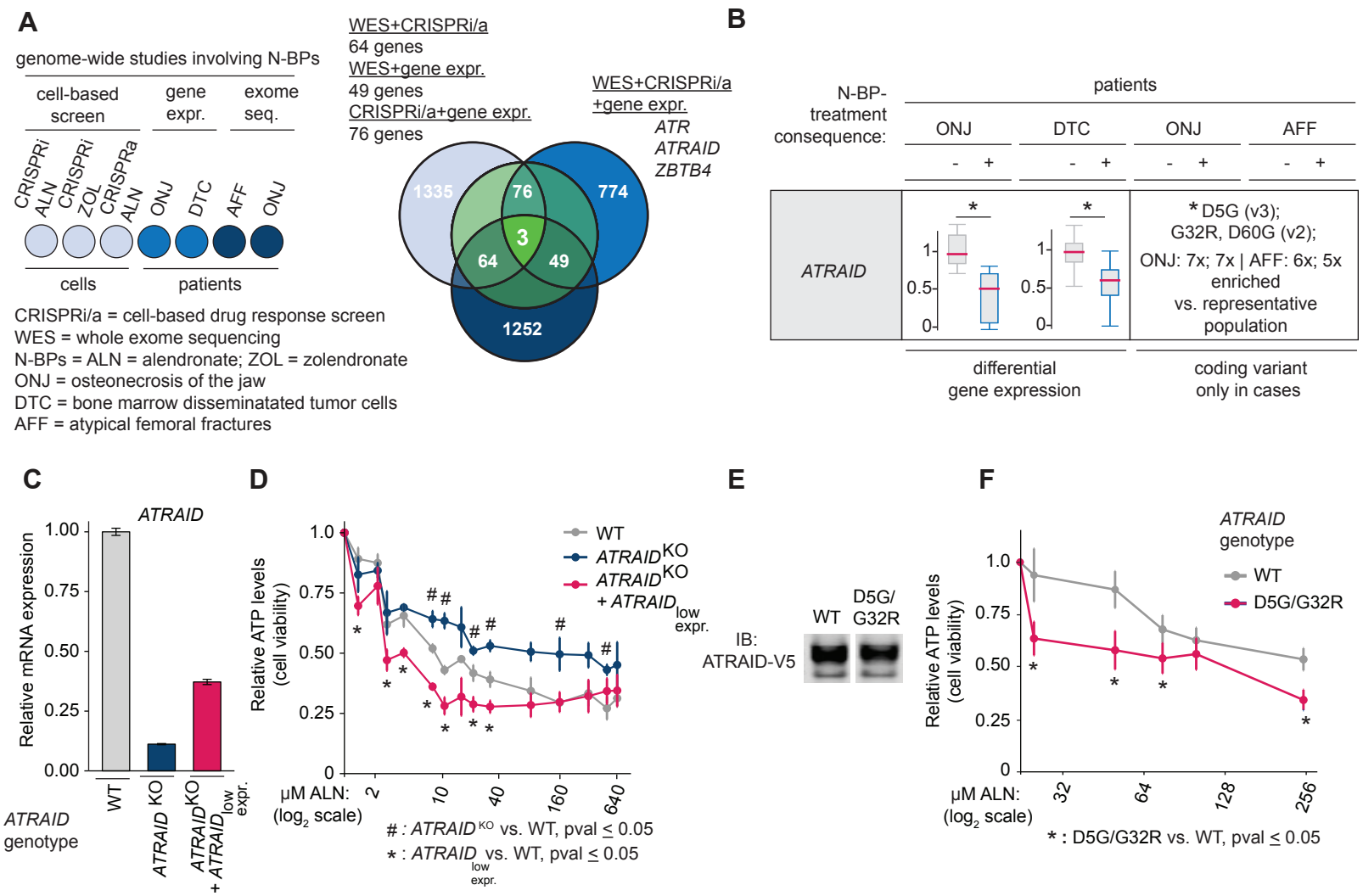
A
genome-wide studies involving N-BPs
cell-based screen
gene expr.
exome seq.
CRISPRi ALN
CRISPRi ZOL
CRISPRa ALN
ONJ
DTC
AFF
ONJ
cells
patients
CRISPRi/a = cell-based drug response screen
WES = whole exome sequencing
N-BPs = ALN = alendronate; ZOL = zolendronate
ONJ = osteonecrosis of the jaw
DTC = bone marrow disseminatated tumor cells
AFF = atypical femoral fractures
WES+CRISPRi/a
64 genes
WES+gene expr.
49 genes
CRISPRi/a+gene expr.
76 genes
WES+CRISPRi/a +gene expr.
ATR
ATRAID
ZBTB4
1335
76
774
3
64
49
1252
B
N-BP-treatment consequence:
patients
ONJ
DTC
ONJ
AFF
- +
ATRAID
* D5G (v3); G32R, D60G (v2);
ONJ: 7x; 7x | AFF: 6x; 5x enriched vs. representative population
differential gene expression
coding variant only in cases
C
ATRAID
Relative mRNA expression
1.00
0.75
0.50
0.25
0.00
WT
ATRAID KO
ATRAID KO + ATRAID low expr.
ATRAID genotype
D
Relative ATP levels (cell viability)
WT
ATRAID KO
ATRAID KO + ATRAID low expr.
μM ALN: (log2 scale)
2
10
40
160
640
: ATRAID KO vs. WT, pval ≤ 0.05
* : ATRAID low expr. vs. WT, pval ≤ 0.05
E
WT
D5G/ G32R
IB: ATRAID-V5
F
ATRAID genotype
WT
D5G/G32R
Relative ATP levels (cell viability)
μM ALN: (log2 scale)
32
64
128
256
* : D5G/G32R vs. WT, pval ≤ 0.05

Figure S1

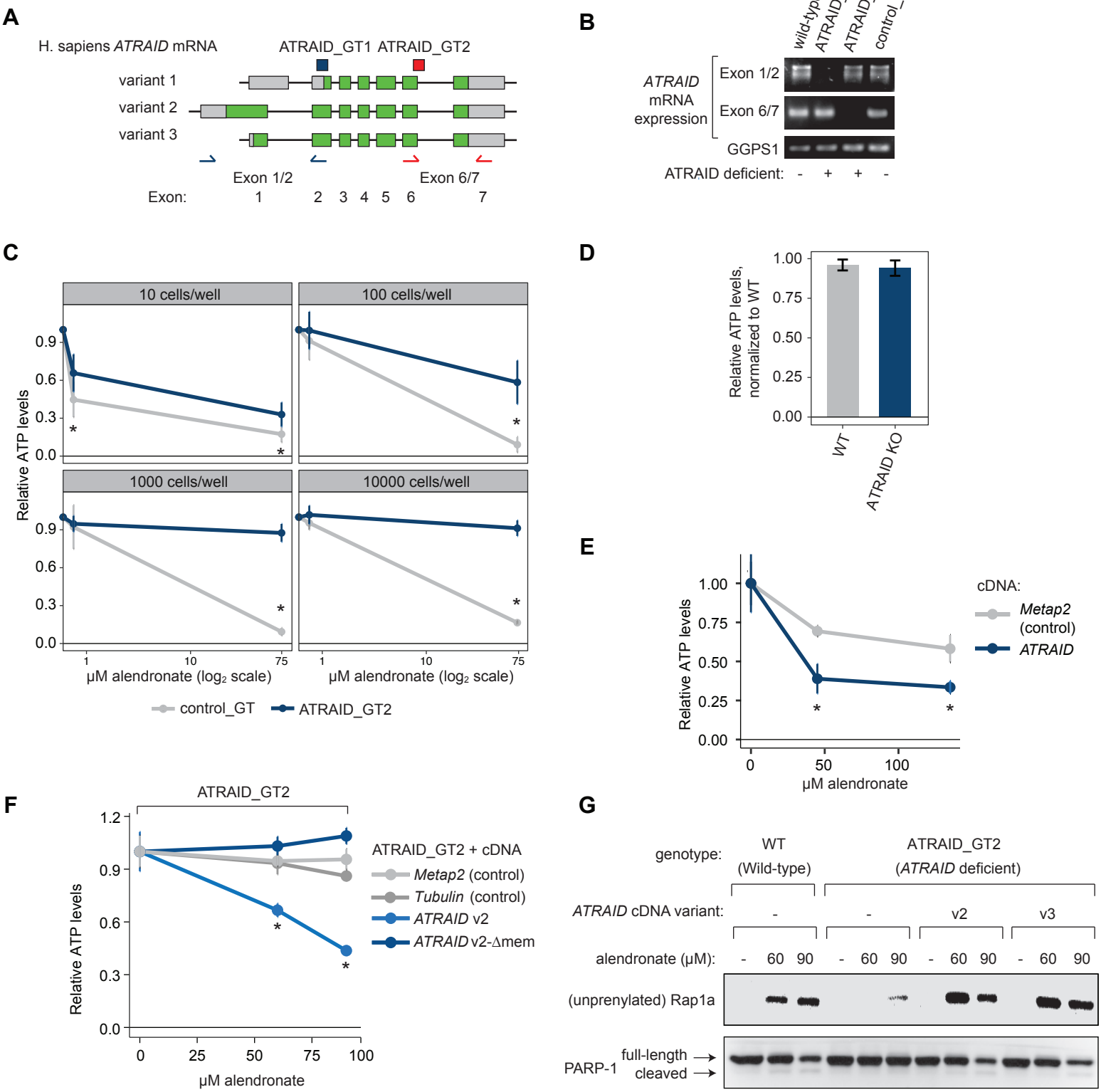
A
H. sapiens ATRAID mRNA
ATRAID_GT1 ATRAID_GT2
variant 1
variant 2
variant 3
Exon 1/2
Exon 6/7
Exon: 1 2 3 4 5 6 7
B
wild-type
ATRAID_GT1
ATRAID_GT2
control_GT1
ATRAID mRNA expression
Exon 1/2
Exon 6/7
GGPS1
ATRAID deficient: - + + -
C
10 cells/well
100 cells/well
1000 cells/well
10000 cells/well
Relative ATP levels
μM alendronate (log2 scale)
control_GT
ATRAID_GT2
D
Relative ATP levels, normalized to WT
WT
ATRAID KO
E
Relative ATP levels
μM alendronate
cDNA:
Metap2 (control)
ATRAID
F
ATRAID_GT2
Relative ATP levels
μM alendronate
ATRAID_GT2 + cDNA
Metap2 (control)
Tubulin (control)
ATRAID v2
ATRAID v2-Δmem
G
genotype:
WT (Wild-type)
ATRAID_GT2 (ATRAID deficient)
ATRAID cDNA variant:
alendronate (μM):
(unprenylated) Rap1a
PARP-1
full-length
cleaved

Figure S2

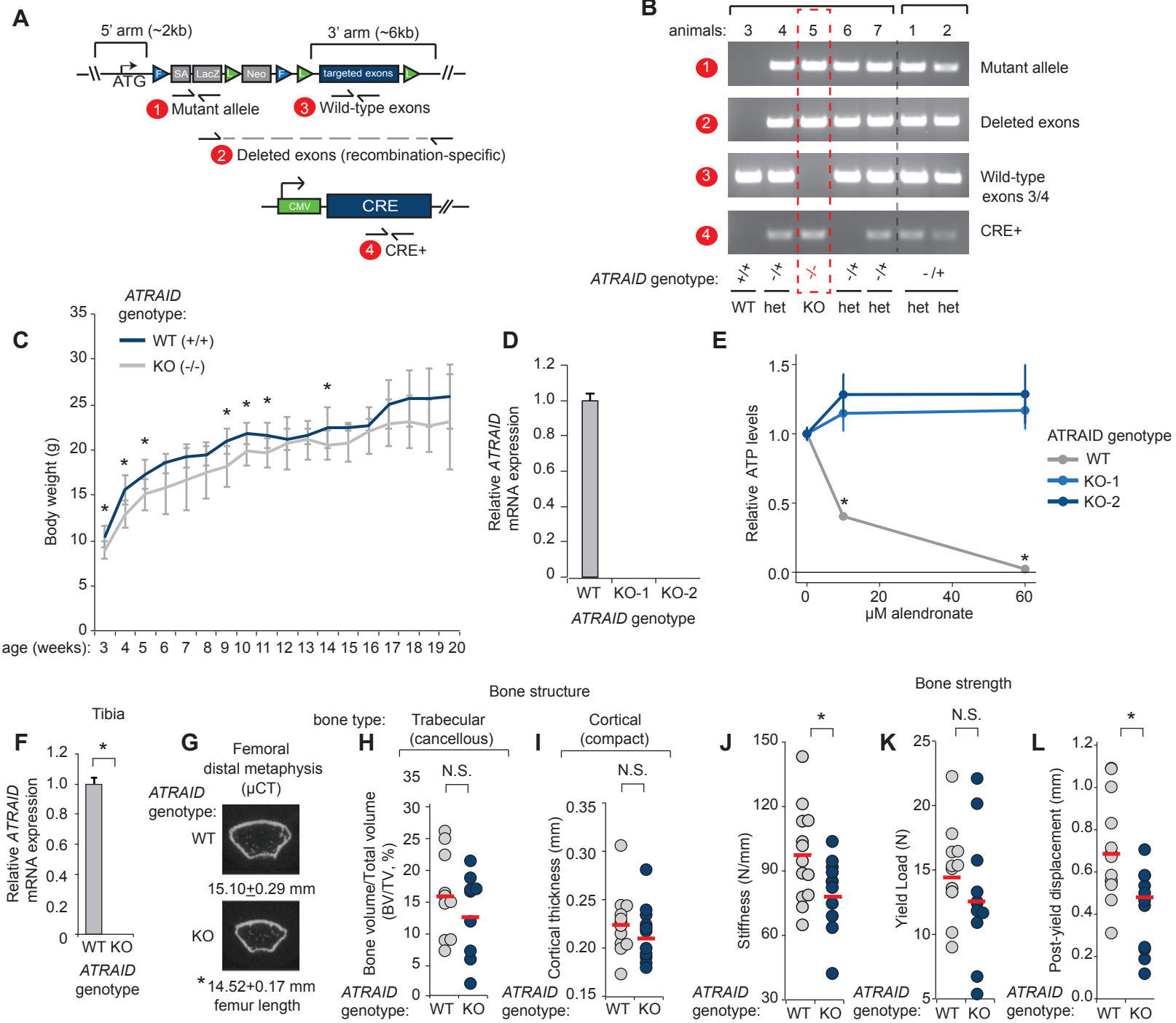
A
5' arm (~2kb)
3' arm (~6kb)
ATG
SA
LacZ
Neo
targeted exons
1 Mutant allele
3 Wild-type exons
2 Deleted exons (recombination-specific)
CMV
CRE
4 CRE+
B
Offspring (F1)
Parents
animals: 3 4 5 6 7 1 2
Mutant allele
Deleted exons
Wild-type exons 3/4
CRE+
ATRAID genotype: +/+ -/+ -/- -/+ -/+ - /+
WT het KO het het het het
C
ATRAID genotype:
WT (+/+)
KO (-/-)
Body weight (g)
age (weeks): 3 4 5 6 7 8 9 10 11 12 13 14 15 16 17 18 19 20
D
Relative ATRAID mRNA expression
WT KO-1 KO-2
ATRAID genotype
E
Relative ATP levels
μM alendronate
ATRAID genotype
WT
KO-1
KO-2
Tibia
F
Relative ATRAID mRNA expression
WT KO
ATRAID genotype
G
Femoral distal metaphysis (μCT)
ATRAID genotype:
WT
15.10±0.29 mm
KO
14.52±0.17 mm
femur length
Bone structure
bone type:
Trabecular (cancellous)
Cortical (compact)
H
N.S.
Bone volume/Total volume (BV/TV, %)
I
N.S.
Cortical thickness (mm)
Bone strength
J
Stiffness (N/mm)
K
N.S.
Yield Load (N)
L
Post-yield displacement (mm)
ATRAID genotype:
WT KO

Figure S2 (continued)

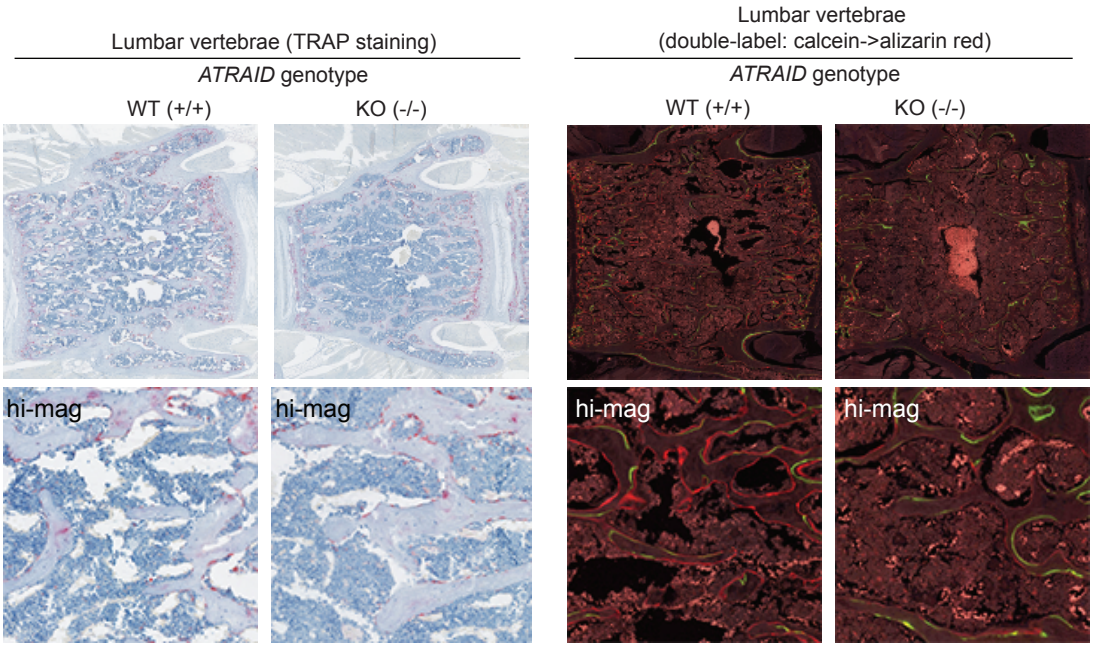

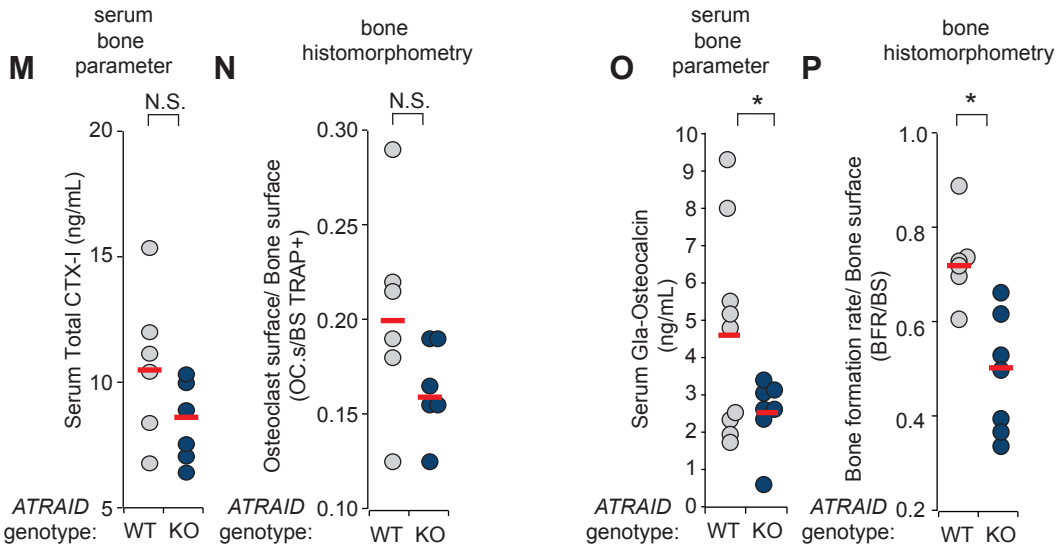

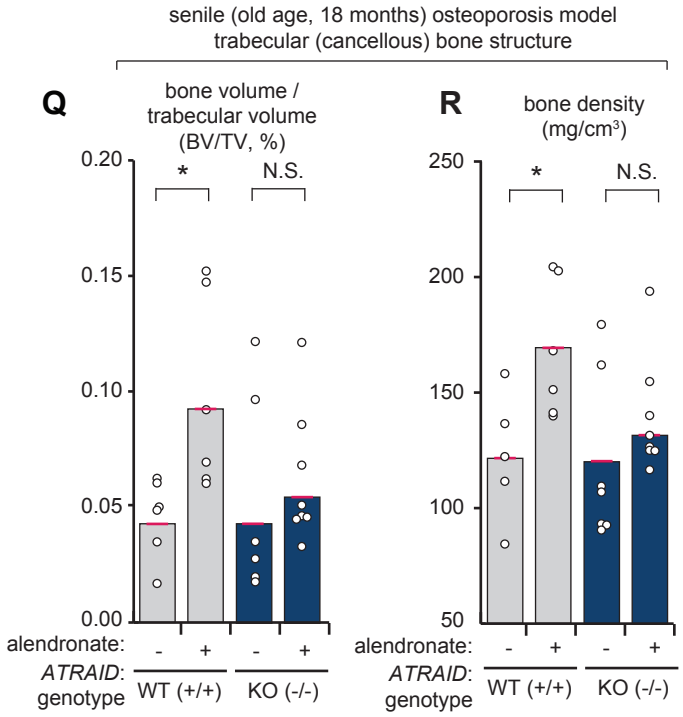

Figure S3

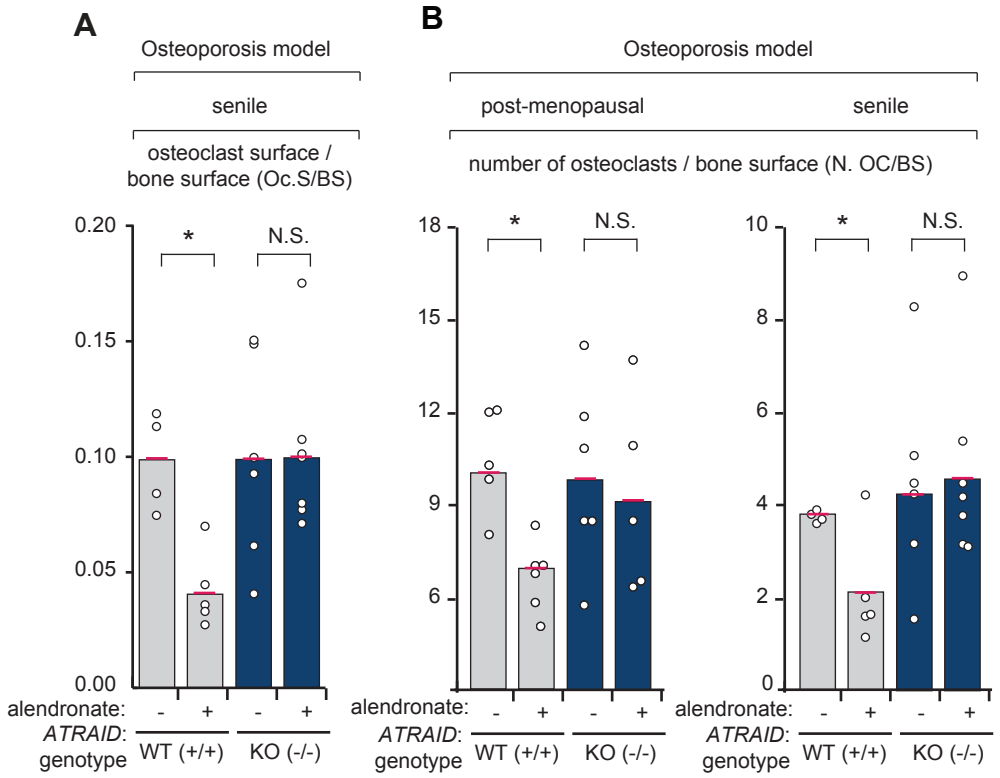
A
Osteoporosis model
senile
osteoclast surface / bone surface (Oc.S/BS)
0.20
0.15
0.10
0.05
0.00
*
N.S.
alendronate: - + - +
ATRAID: genotype WT (+/+) KO (-/-)
B
Osteoporosis model
post-menopausal
senile
number of osteoclasts / bone surface (N. OC/BS)
18
15
12
9
6
10
8
6
4
2
0
*
N.S.
alendronate: - + - +
ATRAID: genotype WT (+/+) KO (-/-)

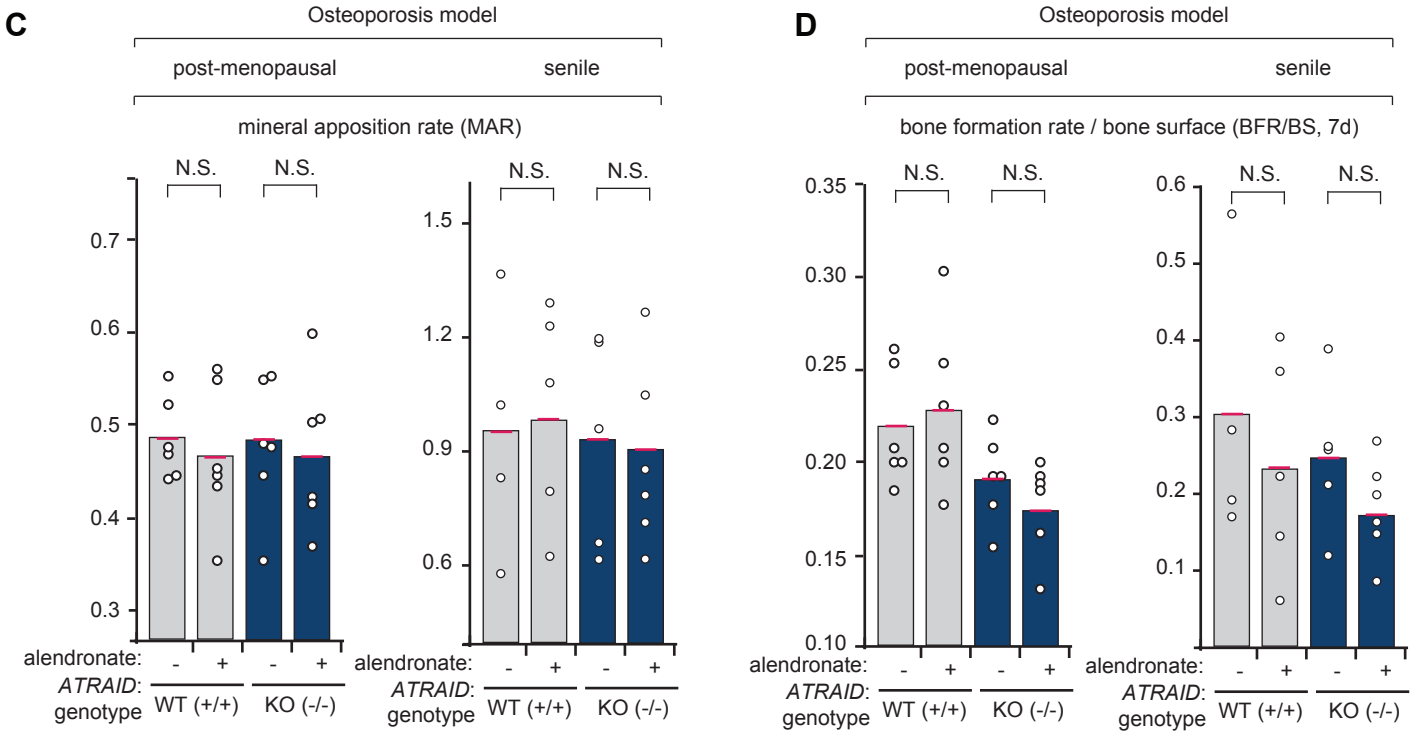
C
Osteoporosis model
post-menopausal
senile
mineral apposition rate (MAR)
0.7
0.6
0.5
0.4
0.3
1.5
1.2
0.9
0.6
N.S.
alendronate: - + - +
ATRAID: genotype WT (+/+) KO (-/-)
D
Osteoporosis model
post-menopausal
senile
bone formation rate / bone surface (BFR/BS, 7d)
0.35
0.30
0.25
0.20
0.15
0.10
0.6
0.5
0.4
0.3
0.2
0.1
N.S.
alendronate: - + - +
ATRAID: genotype WT (+/+) KO (-/-)

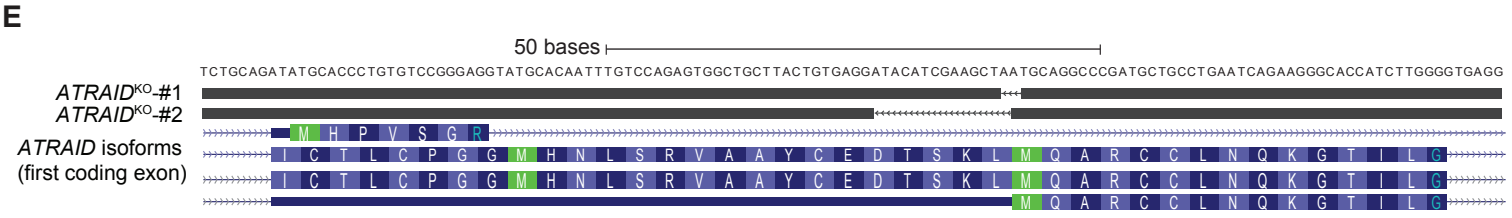
E
50 bases
TCTGCAGATATGCACCCTGTGTCCGGGAGGTATGCACAATTTGTCCAGAGTGGCTGCTTACTGTGAGGATACATCGAAGCTAATGCAGGCCCGATGCTGCCTGAATCAGAAGGGCACCATCTTGGGGTGAGG
ATRAID^KO-#1
ATRAID^KO-#2
ATRAID isoforms (first coding exon)
M H P V S G R
I C T L C P G G M H N L S R V A A Y C E D T S K L M Q A R C C L N Q K G T I L G
I C T L C P G G M H N L S R V A A Y C E D T S K L M Q A R C C L N Q K G T I L G
M Q A R C C L N Q K G T I L G